Electronic Supplementary Materials

Construction of Hierarchically Chiral Metal–Organic Frameworks for Fast and Mild Asymmetric Catalysis

Zahra Sharifzadeh‡, Sayed Ali Akbar Razavi, ‡ and Ali Morsali *

Department of Chemistry, Faculty of Sciences, Tarbiat Modares University, P.O. Box 14117-13116, Tehran, Islamic Republic of Iran

‡ These two authors contributed equally in this work.

Section S1. Materials and Methods. All starting materials for the synthesis were purchased from commercial providers and used without further purification (Sigma-Aldrich, Merck and the others). **FT-IR** spectra were recorded using a Nicolet Fourier Transform IR, Nicolet 100 spectrometer in the range 400-4000 cm-1 using the KBr disk technique. X-ray powder diffraction (**PXRD**) measurements were performed using a Philips X'pert diffractometer with monochromated Cu-Kα (λ=1.54056 A) radiation. The N2 adsorption/desorption isotherm was measured at 77 K using a Micromeritics ASAP 2020 analyzer. The specific surface area was calculated by the Brunauer-Emmett-Teller (**BET**) method. The samples were characterized with by scanning electron microscopy (**SEM**) ZEISS SIGMA VP (Germany) with gold coating. The samples were characterized using energy dispersive X-ray spectroscopy (**EDAX**) on a CamScan MV2300 instrument with gold coating. Echrom **GC** A90 gas chromatography with a flame-ionization detector (China) was employed (Agilent HP-5 capillary column, 30 m × 0.320 mm × 0.25 μm, temperature limits from 60 °C to 325 °C) for the symmetric reactions products. For determining the enantiomeric excess (ee), a **chiral column** was used (Agilent CYCLODEX-B capillary column, 30 m × 0.25 mm × 0.25 μm, temperature limits from 50 °C to 230 °C).

Section S2. Structural Characterization

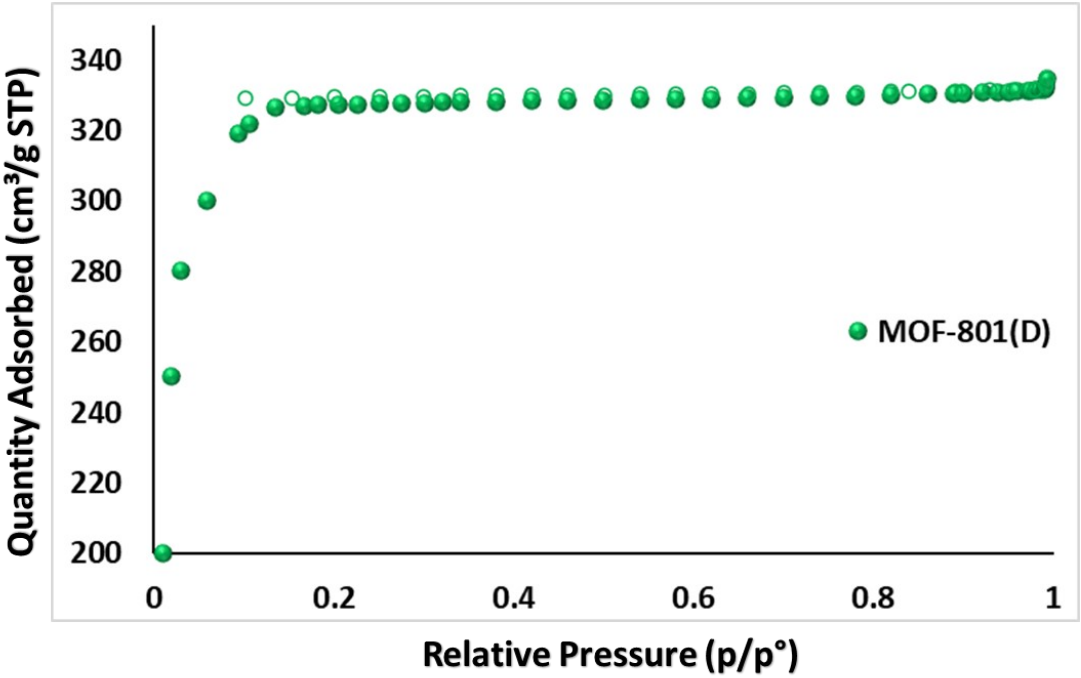

Figure S1. N_2 sorption isotherms of MOF-801(D) at 77 K.

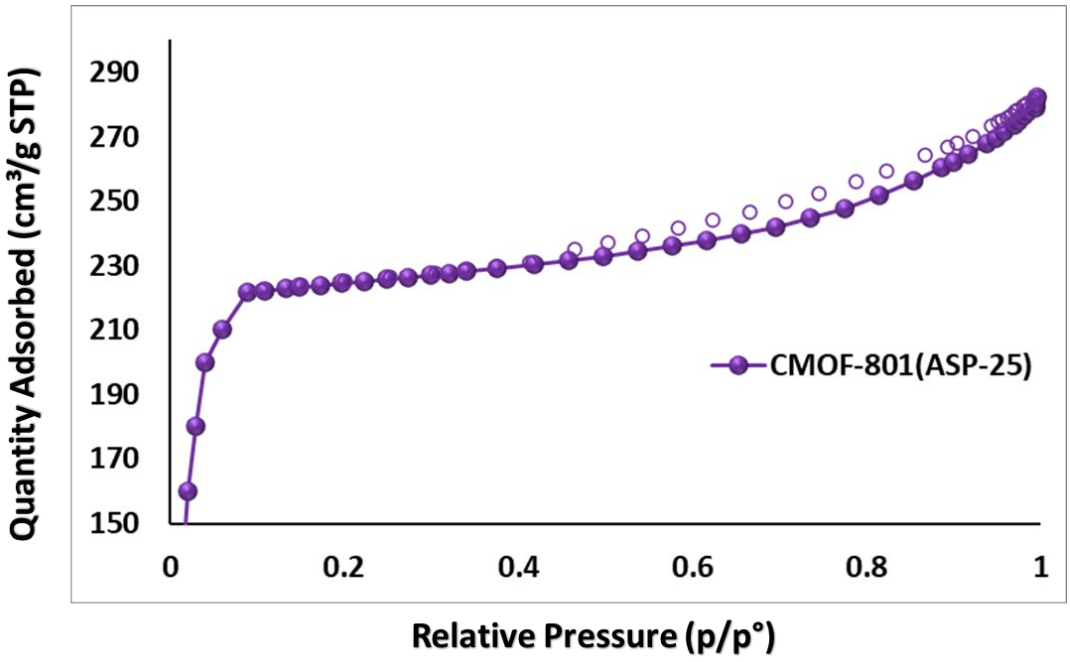

Figure S2. N_2 sorption isotherms of CMOF-801(ASP-25) at 77 K, showing hysteresis loop.

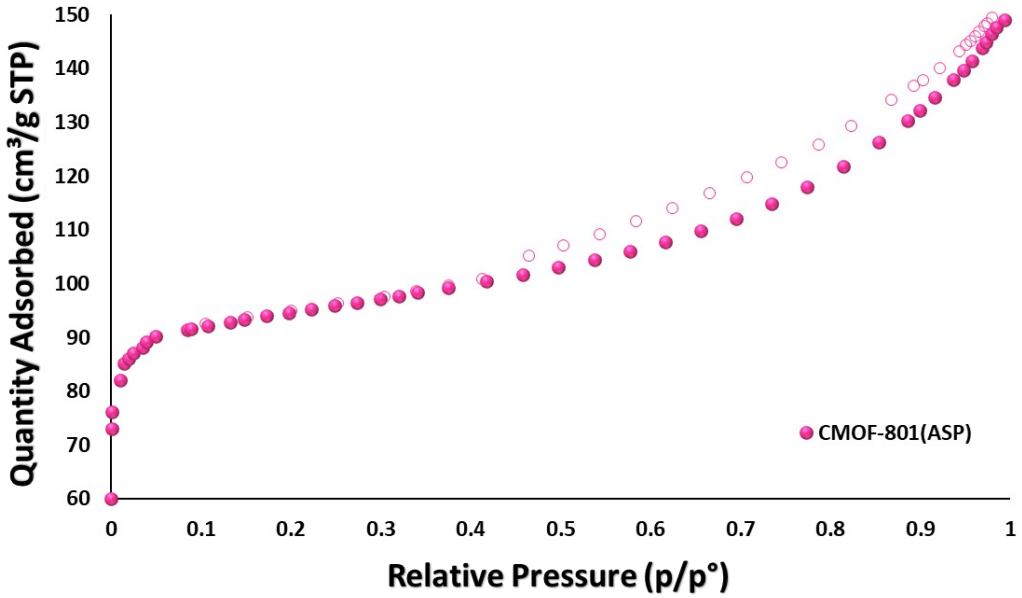

Figure S3. N_2 sorption isotherms of CMOF-801(ASP) at 77 K, showing hysteresis loop.

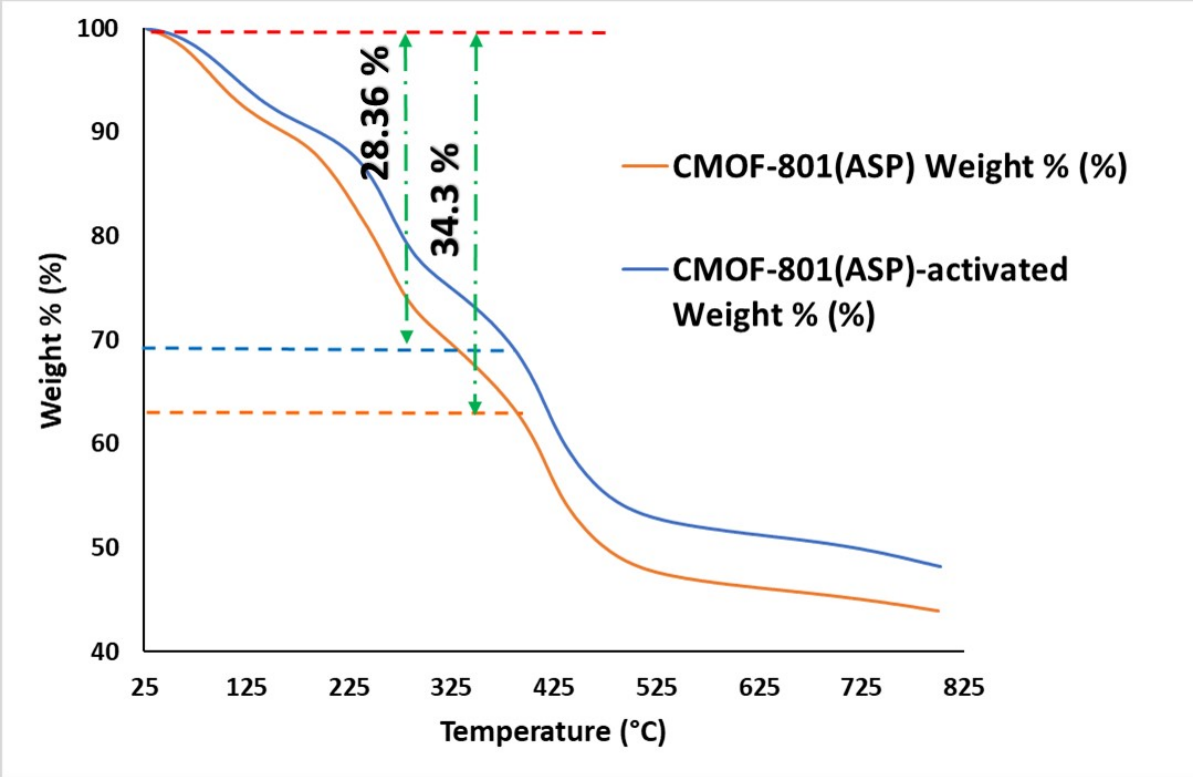

Figure S4. TGA curves of the CMOF-801(ASP) obtained before and after activation treatment for confirmation of generated defect sites, measured under 15 °C/min heating rate and N_2 carrier gas flow.

Calculation of fumarate and aspartate ligands in CMOF-801(ASP)

The total weight loss in wt.% between 190°C (ligand containing state) and 519 °C (ligands are decomposed) for CMOF-801(ASP) was calculated to be 41.22%.

The detailed calculations are;

CMOF-801(ASP): (90.94-53.45)/90.94 = 41.22 %

By taking into account, one of the six ligands is missed, and two aspartic acid present in the formula of the dehydrated MOF-801 to form a defect structure, theoretical loss of all ligands to be calculated as follows:

$Zr_6O_6(O_2C\text{-}(CH)_2\text{-}CO2)_3(O_2C\text{-}(CH_2)\text{-}(CHNH_2)\text{-}CO_2)_2$ [M.W= 1257.73]

MW of $(ZrO_2)_6$ = 739.272

Then estimated weight loss will be: (1257.73-739.272)/1257.73 = 41.22 %

Therefore, we can estimate that almost 1/6 ligand of its perfect crystal structure was missed in CMOF-801(ASP), and two aspartic acid were substitued in the two fumaric acid position.

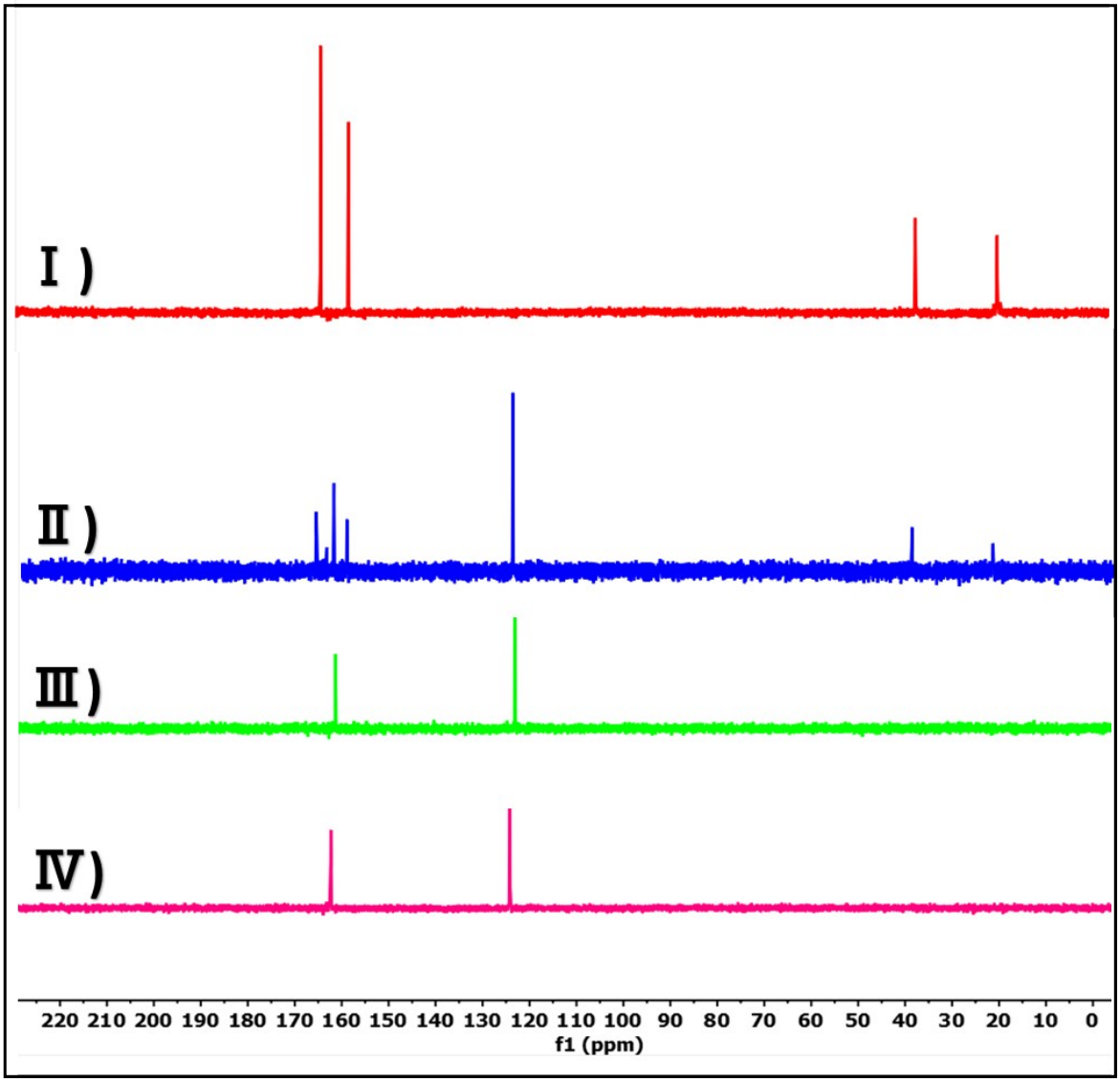

Figure S5. ^{13}CNMR of (I) L-Aspartic acid, (II) CMOF-801(ASP), (III) Fumaric acid (IV) MOF-801(D)

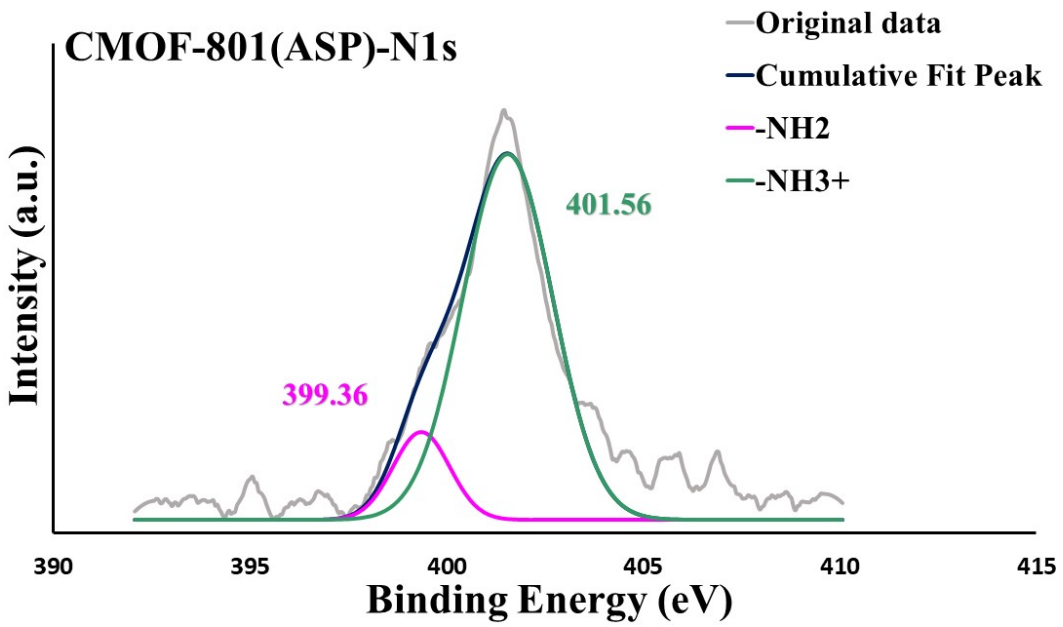

Figure S6. XPS spectra of N1s in CMOF-801(ASP), clarified high density of NH_3^+ relative to NH_2.

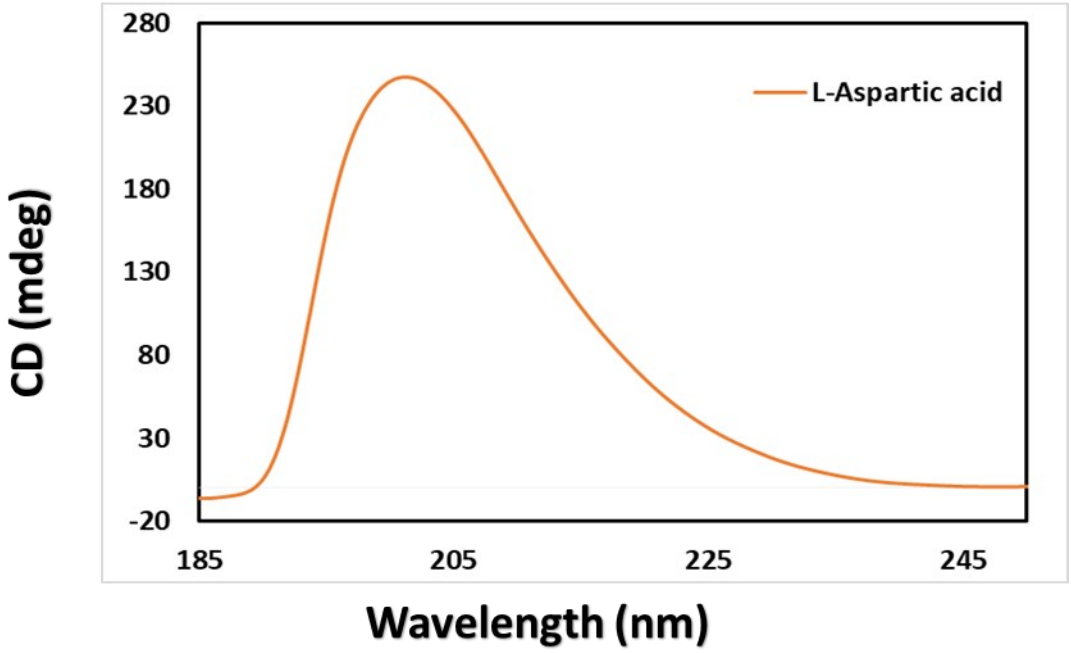

Figure S7. Circular dichroism (CD) spectra of (a) pure L-aspartic acid in aqueous solution.

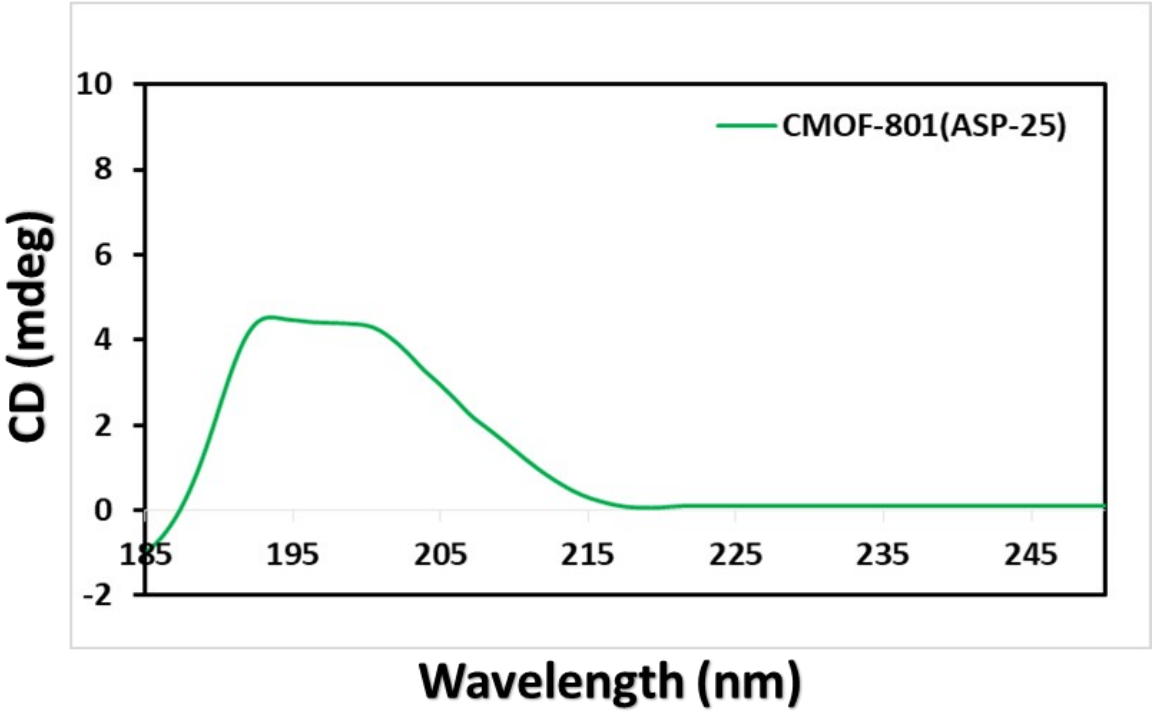

Figure S8. Circular dichroism (CD) spectra of (a) CMOF-801(ASP-25) dispersed in aqueous solution

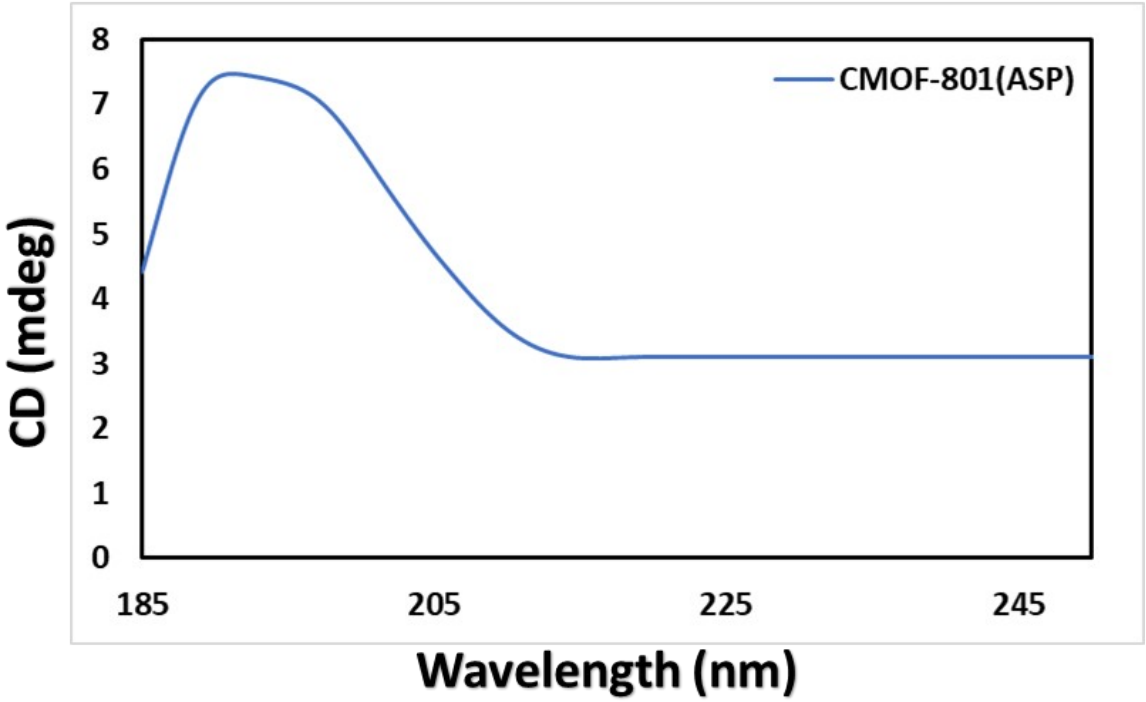

Figure S9. Circular dichroism (CD) spectra of (a) CMOF-801(ASP) dispersed in aqueous solution.

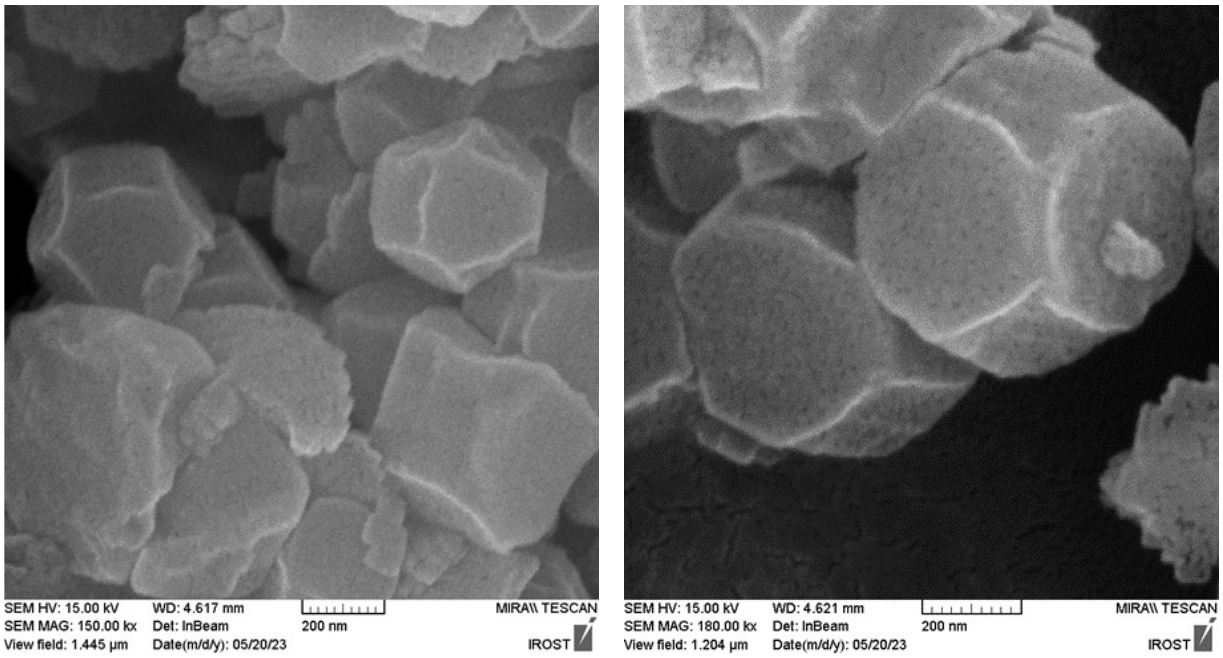

Figure S10. SEM images for MOF-801(D).

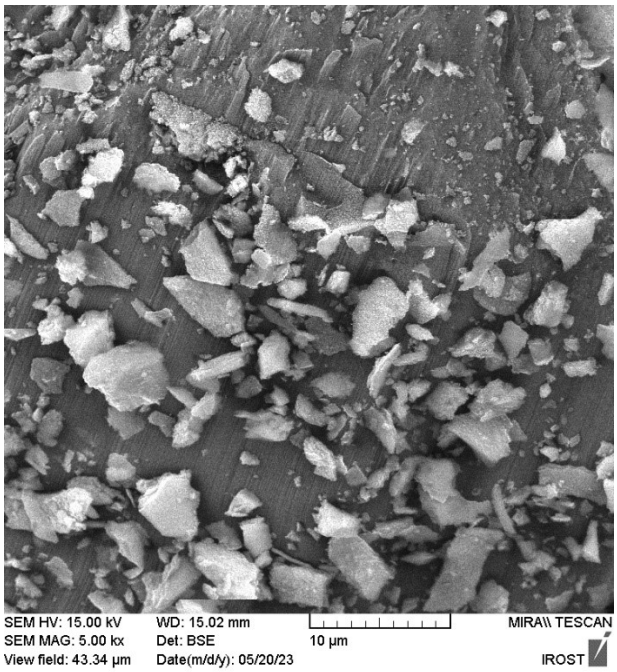

Figure S11. SEM images for CMOF-801(ASP).

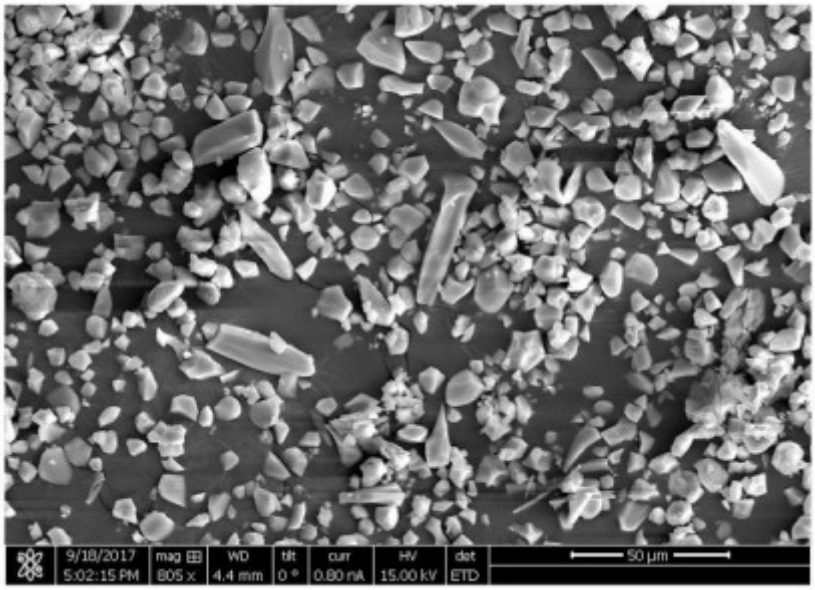

Figure S12. SEM images of MIP-202(Zr) sample obtained from reaction without stirring. with permission from [1].

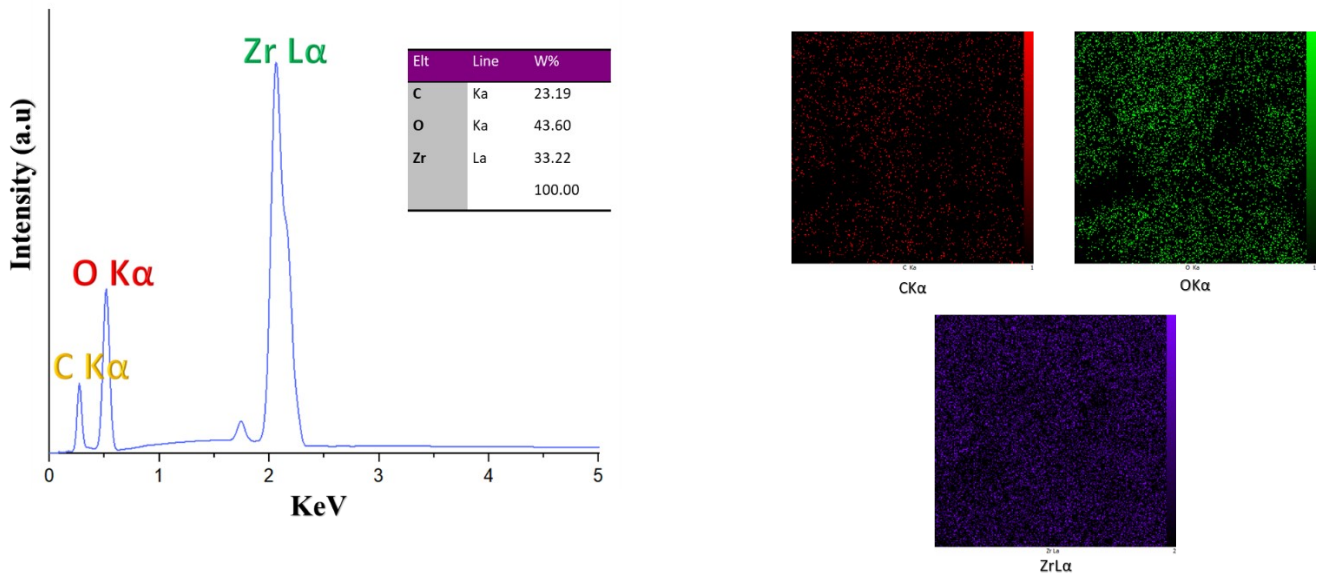

Figure S13. EDS spectra, and SEM-EDX elemental mapping of MOF-801(D).

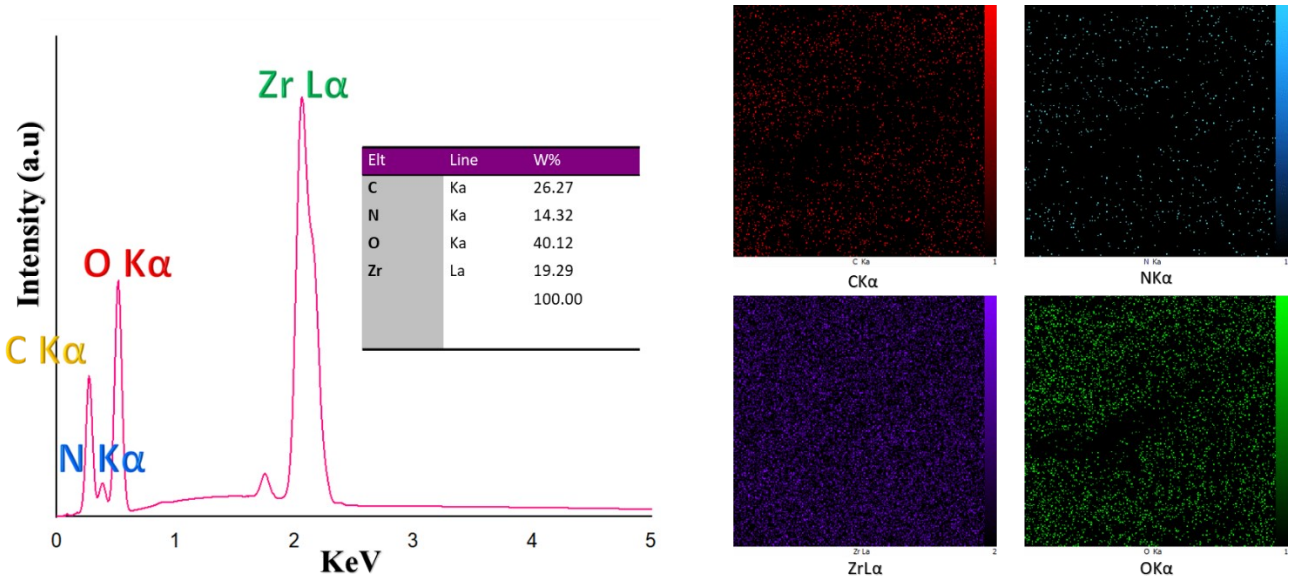

Figure S14. EDS spectra, and SEM-EDX elemental mapping of CMOF-801(ASP).

Section S3. Ring-opening reaction Characterization

Table S1. Optimization reaction condition for Ring-opening reaction

Entry	Catalyst	Temperature (ºC)	Time	Conversion (%)	Ee (%)
1	MOF-801(P)	R.T	5 minutes	2	-
2	MOF-801(P)	50ºC	24 hour	20	-
3	MOF-801(D)	R.T	5 minutes	83	-
4	CMOF-801(ASP-25)	R.T	5 minutes	90	R
4	CMOF-801(ASP)	R.T	5 minutes	100	R
5	Fumaric acid	R.T	5 minutes	5	-
6	L-Aspartic acid	R.T	5 minutes	8	R
7	$ZrCl_4$	R.T	5 minutes	5>	-
8	Physical mixture of L-ASP& $ZrCl_4$	R.T	5 minutes	10>	-

Table S2. Reaction scope for Ring opening reaction of epoxides with various nucleophiles catalysed in the presence of CMOF-801(ASP) as a heterogeneous catalyst[a]

Entry	Alcohol	Epoxide	Product	Conversion (%)[b]
1	Methanol	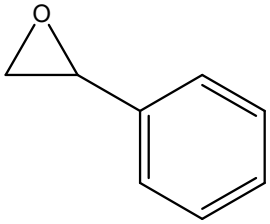	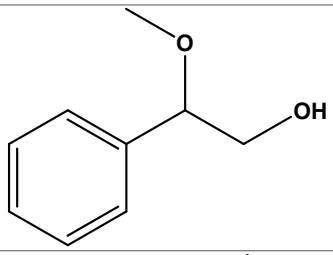	100
2	Ethanol	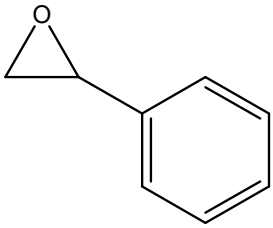	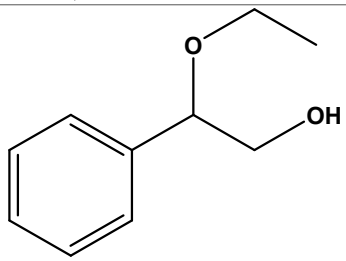	48[c]
3	2-propanol	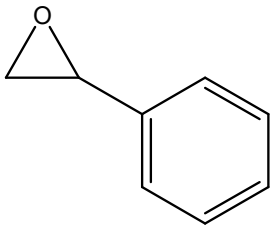	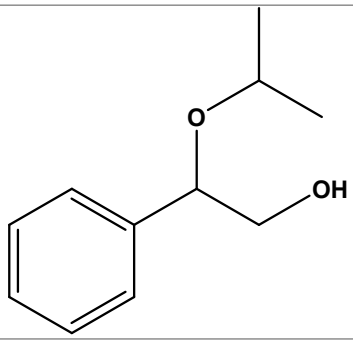	13[c]
4	Methanol	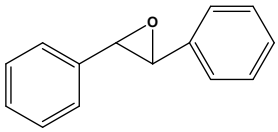	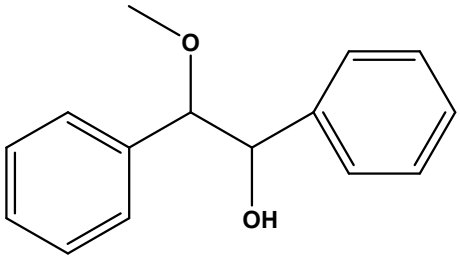	28[c]

[a] Reaction conditions: epoxide (30 mg), alcohols (2 mL), CMOF-801(ASP) catalyst (5 mg), room temperature, 5 minutes.

[b] Isolated product determined by GC.

[C] In 15 minutes.

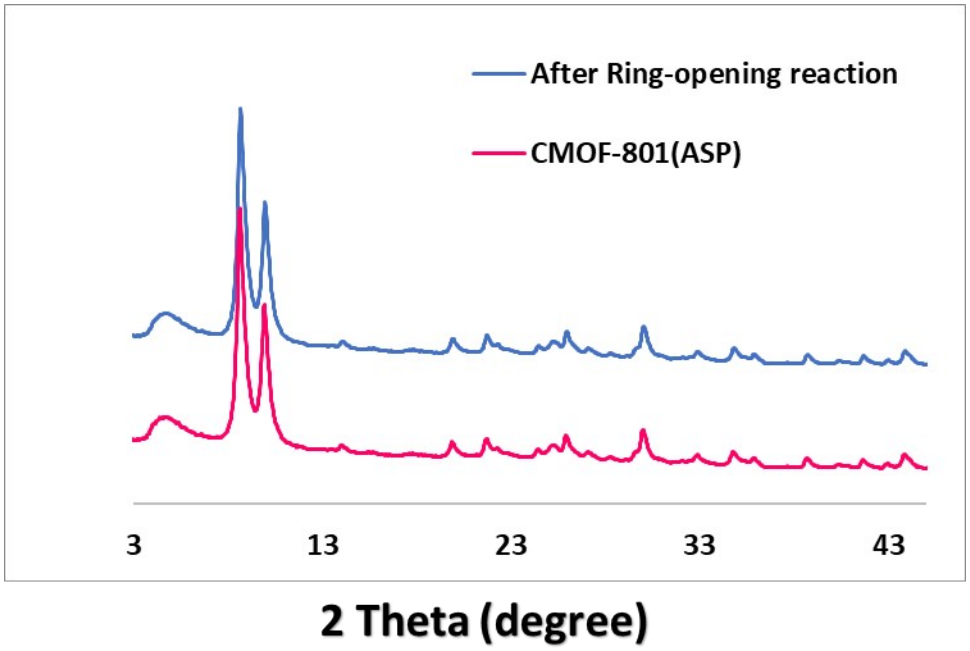

Figure S15. PXRD pattern comparison before and after using of CMOF-801(ASP) chiral catalyst for ring opening reaction.

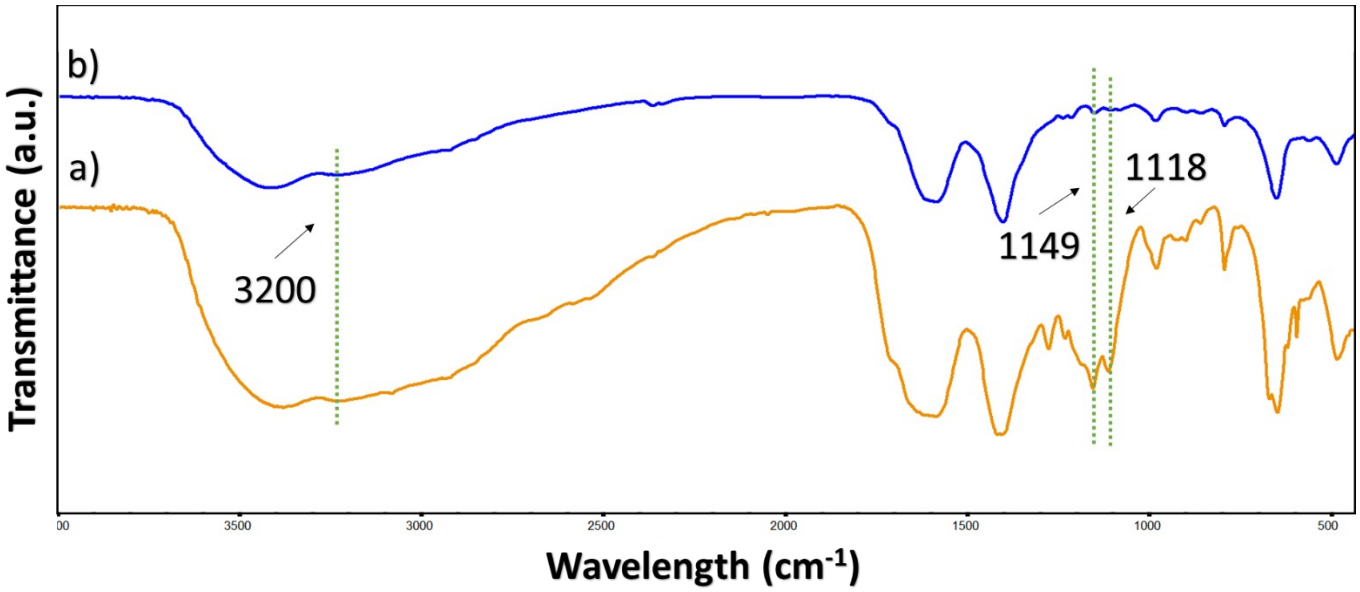

Figure S16. FTIR spectrum comparison (a) before and (b) after using of CMOF-801(ASP) chiral catalyst for ring opening reaction.

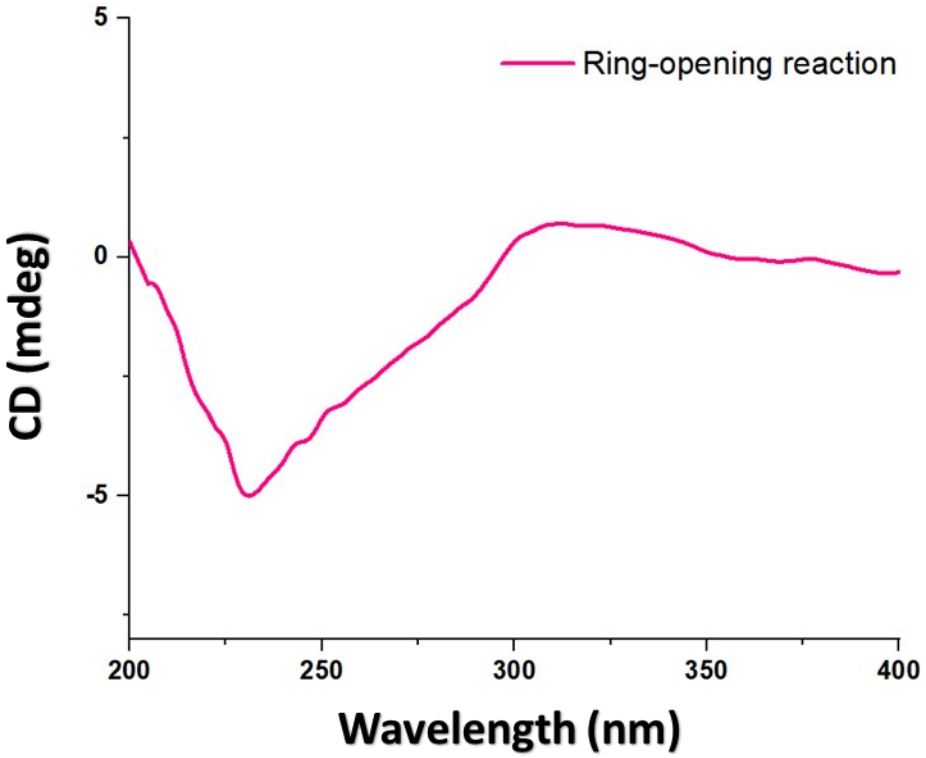

Figure S17. Circular dichroism for characterization of major enantiomer for the ring-opening reaction.

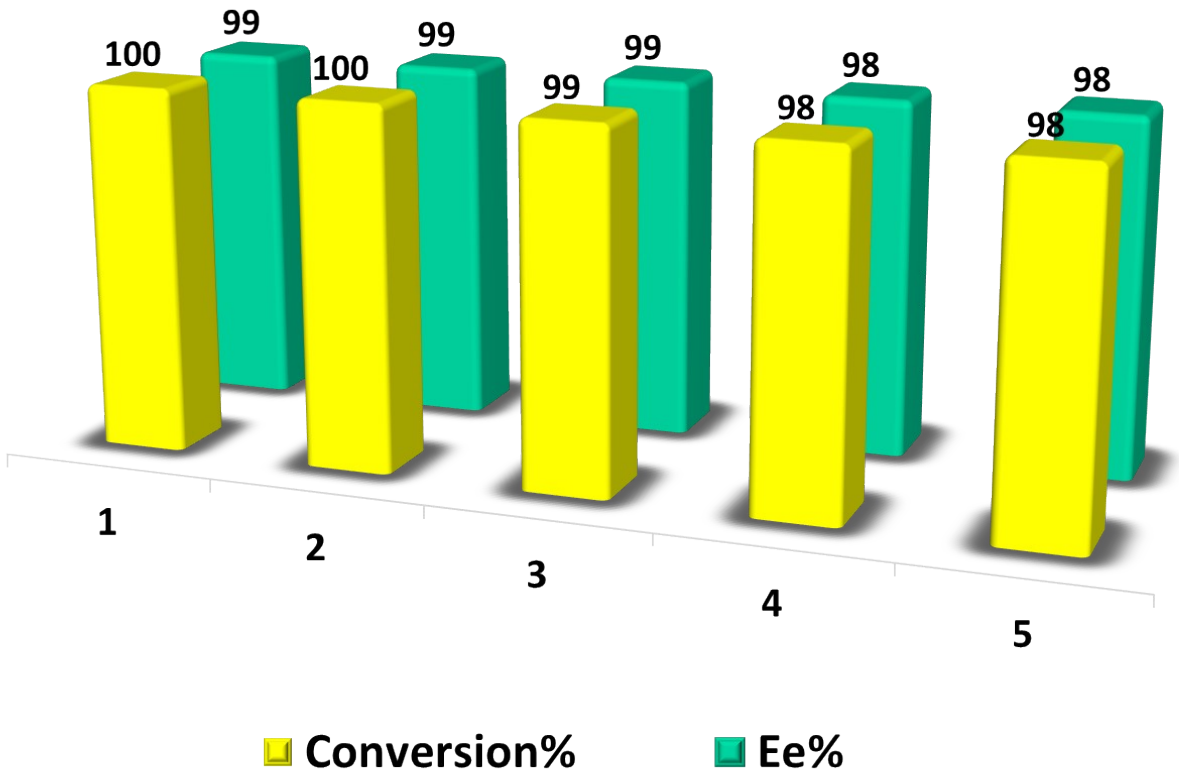

Figure S18. Reusability tests of CMOF-801(ASP) for Ring-opening reaction.

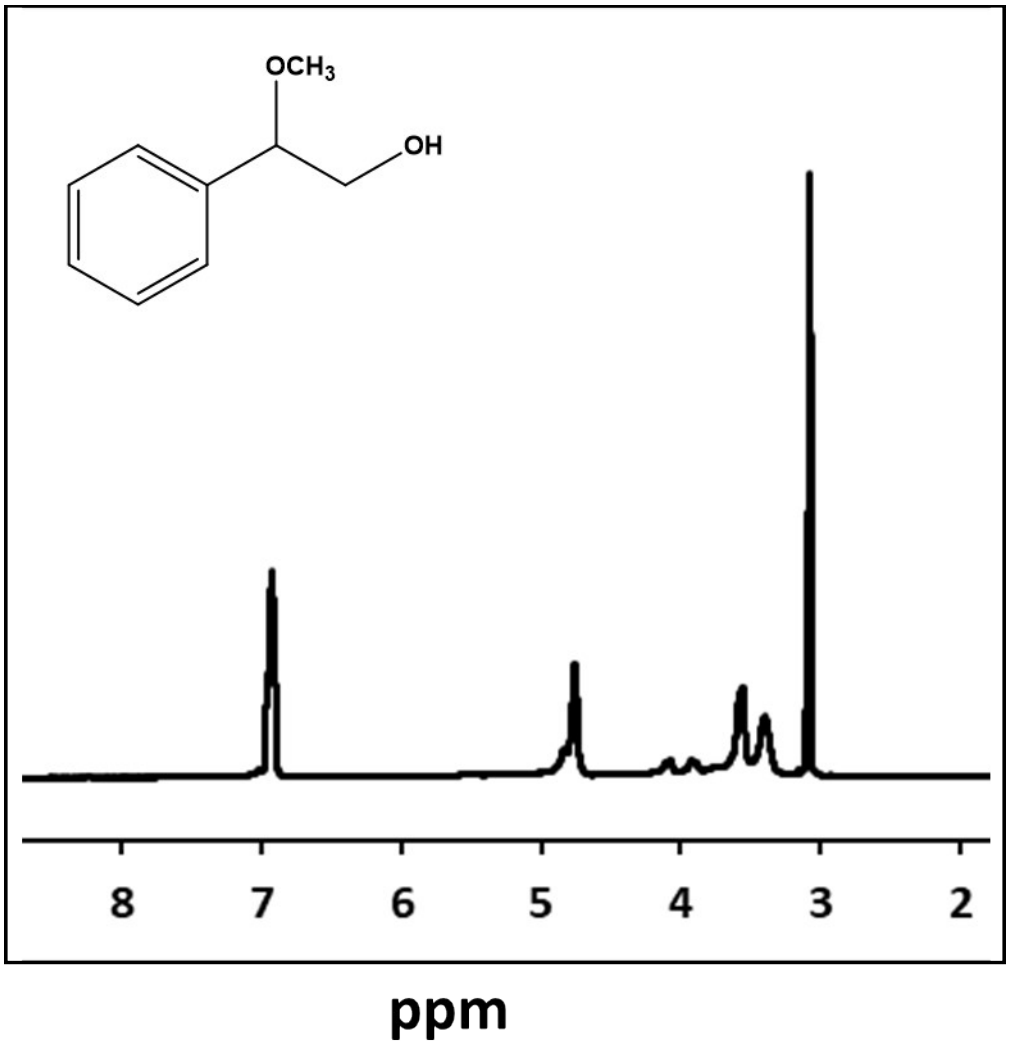

Figure S19. ^{1}H NMR of 2-methoxy-2-phenylethan-1-ol in D_2SO_4.

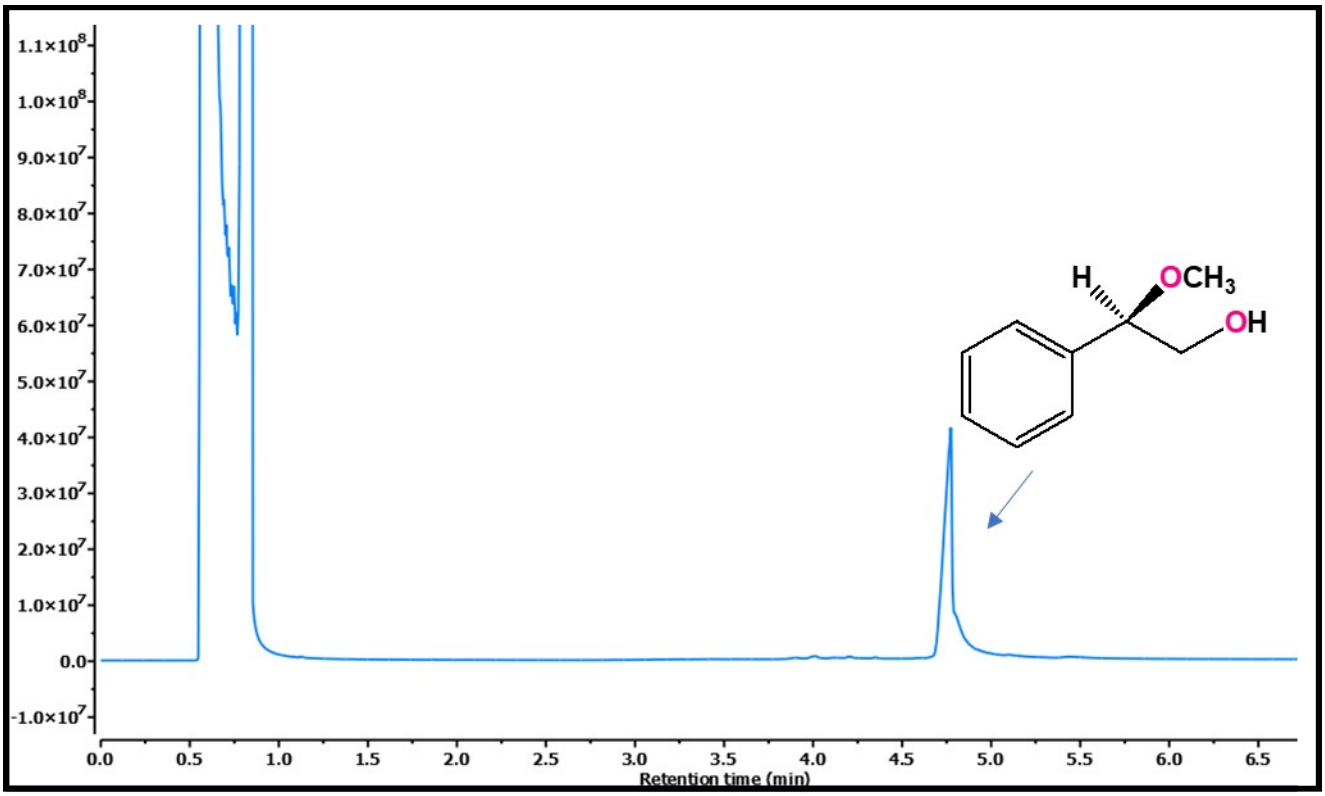

Figure S20. GC chromatogram for the ring-opening of styrene epoxide catalyzed by CMOF-801(ASP)

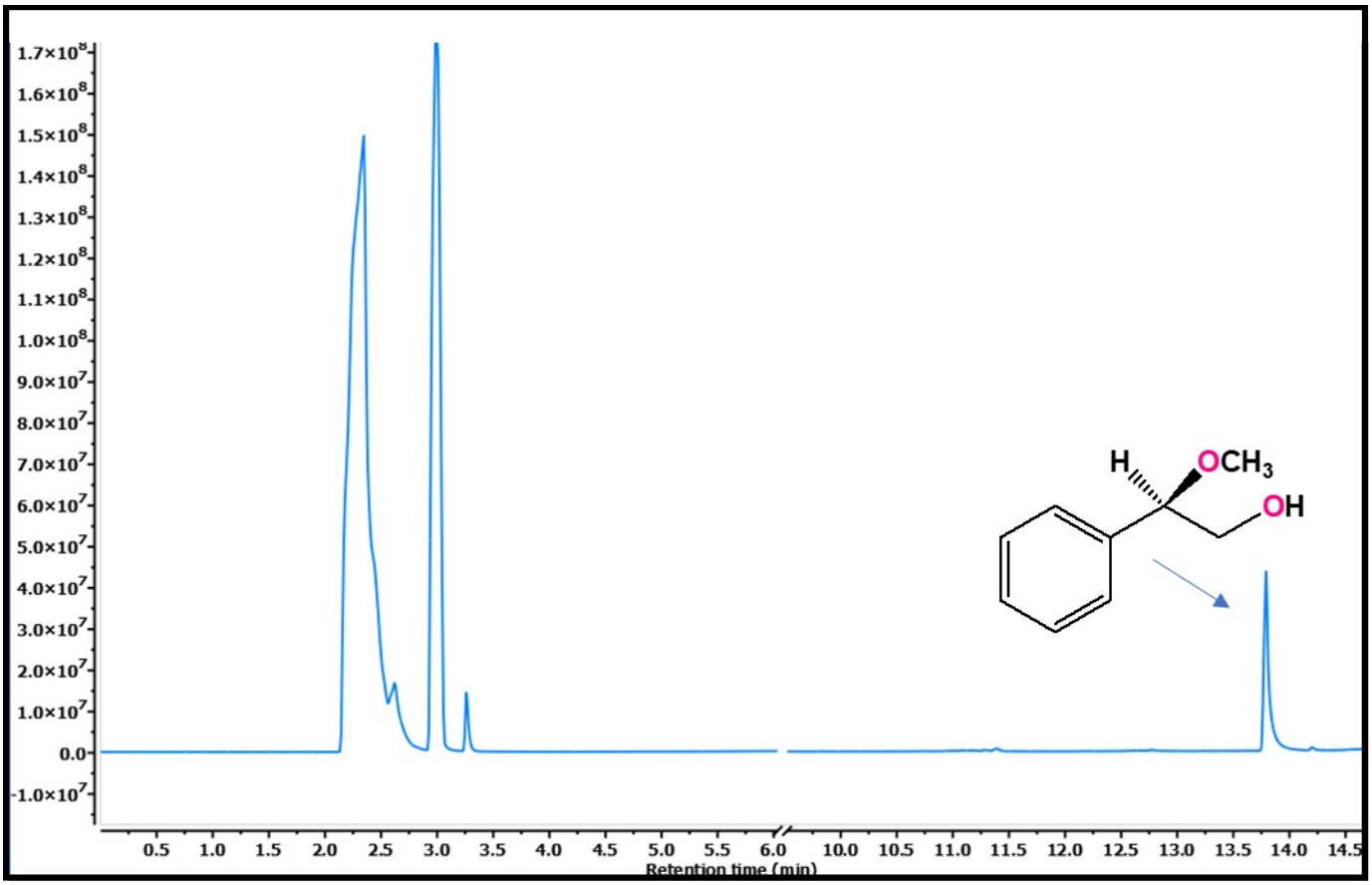

Figure S21. Chiral GC chromatogram for the ring-opening of styrene epoxide catalyzed by CMOF-801(ASP)

Table S3. Comparison of CMOF-801-(ASP) with other catalysts in ring-opening reaction for epoxy styrene.

Entry	**Catalyst**	**Temp (ºC)**	**Time**	**Yield (%)**	**Ref.**
1	**UiO-66**	55	12h	100	2
2	**(R)-MOF-1**	60 ºC	24	95	3
3	**(R)-3**	40 ºC	24	48	4
4	**(R)-3**	60 ºC	24	66	4
5	**TMU-50S**	60 ºC	32	98	5
6	**MOF-801(P)**	R.T	5 minuets	10	**This work**
7	**MOF-801(D)**	R.T	5 minuets	83	**This work**
8	**MOF-801(ASP)**	R.T	5 minuets	100	**This work**

Section S4. Henry reaction Characterization

Table S4. Optimization reaction condition for Henry reaction.

Entry	Catalyst	Temperature (ºC)	Time	Conversion (%)	Ee (%)
1	MOF-801(P)	R.T	24 hour	15	-
3	MOF-801(D)	R.T	5 minutes	89	-
4	CMOF-801(ASP-25)	R.T	5 minutes	92	R
4	CMOF-801(ASP)	R.T	5 minutes	100	R
5	Fumaric acid	R.T	5 minutes	N.R	-
6	L-Aspartic acid	R.T	5 minutes	5>	R
7	$ZrCl_4$	R.T	5 minutes	14	-
8	Physical mixture of L-ASP& $ZrCl_4$	R.T	5 minutes	17	-

Table S5. Reaction scope for Henry Reaction with various substituted benzaldehyde and nitromethane catalysed in the presence of CMOF-801(ASP) as a heterogeneous catalyst [a]

Entry	Aldehyde	Solvent	Product	Conversion (%)[b]
1	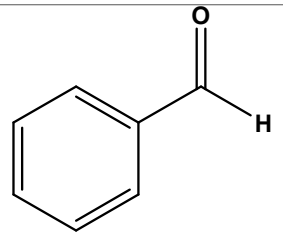	MeOH	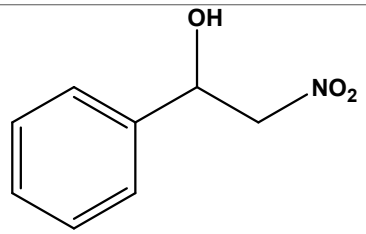	100
2	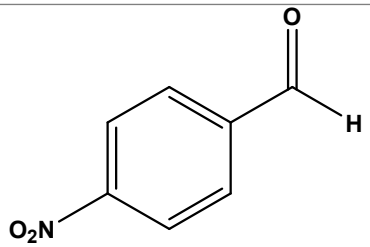	MeOH	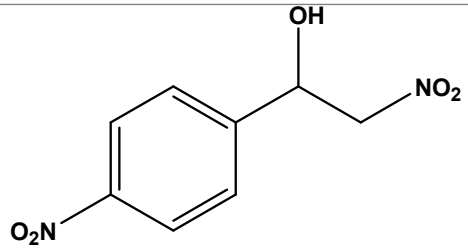	100
3	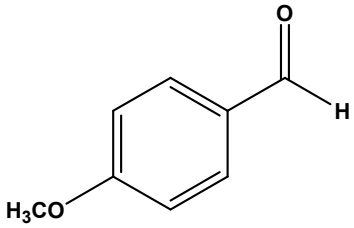	MeOH	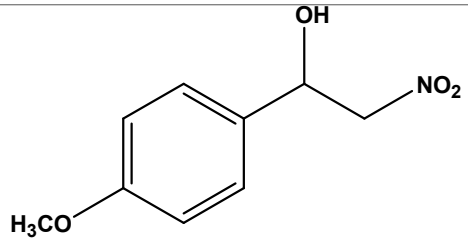	81
4	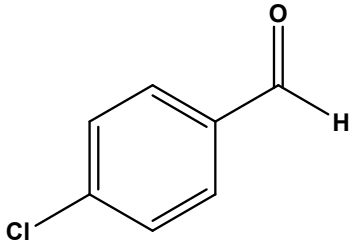	MeOH	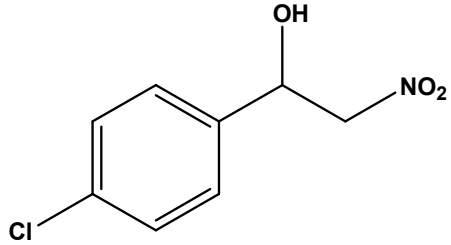	100

[a] Reaction conditions: aldehyde (2 mmol) and nitromethane (5 mmol) in 2 mL of MeOH at room temperature for 15 minutes.

[b] Isolated product determined by GC.

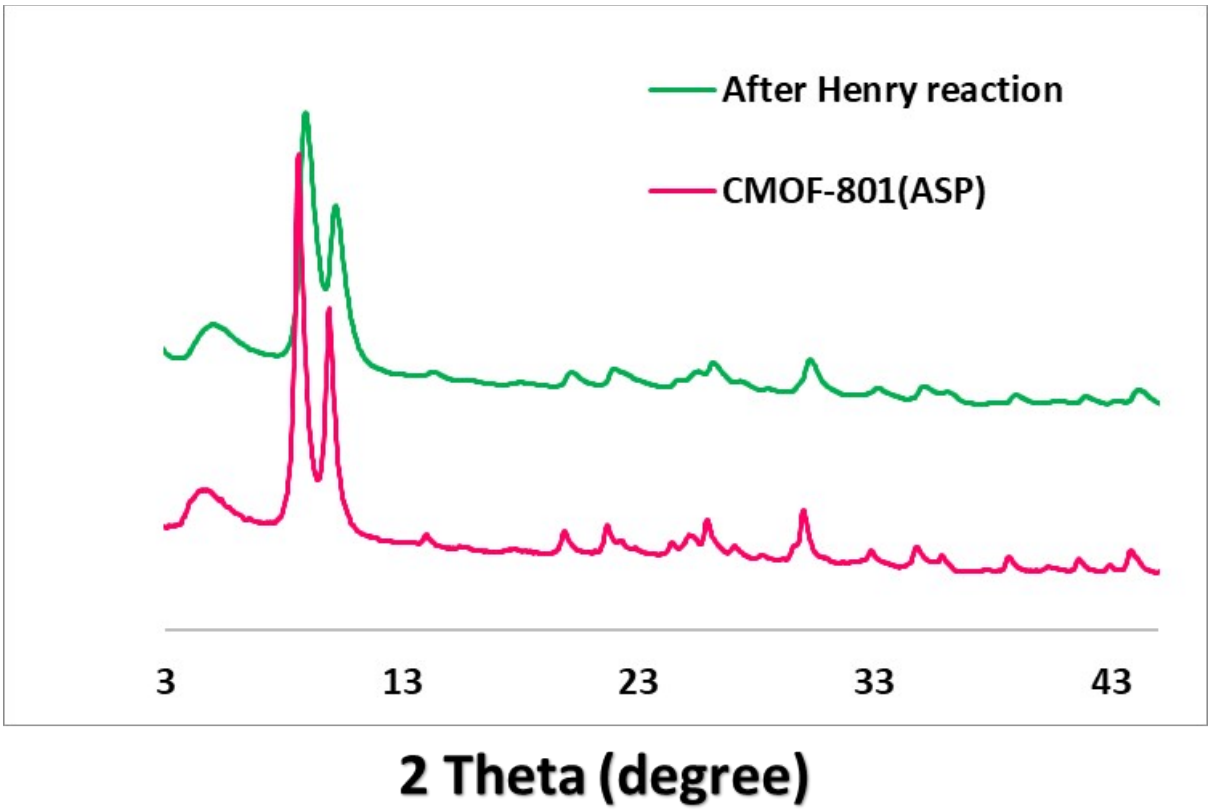

Figure S22. PXRD pattern comparison before and after using of CMOF-801(ASP) chiral catalyst for Henry reaction.

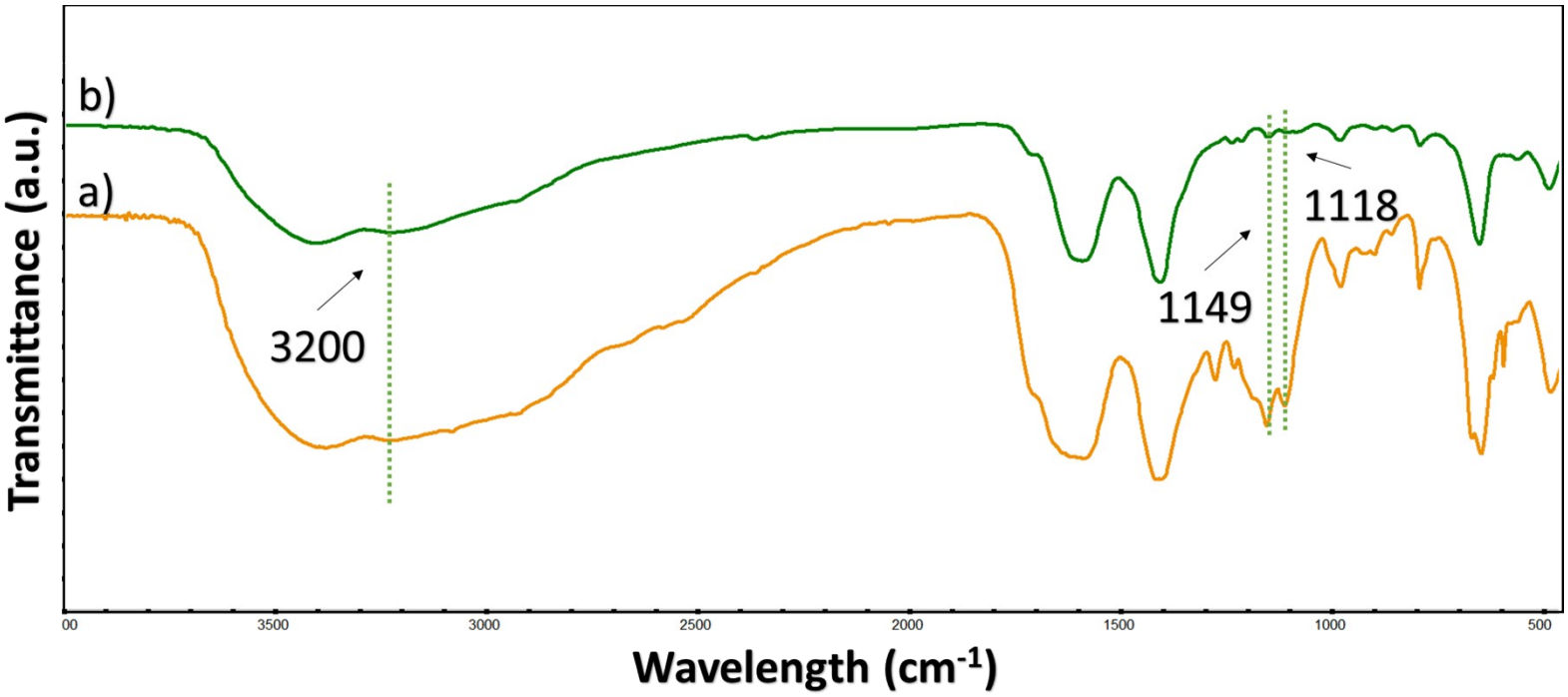

Figure S23. FTIR spectrum comparison (a) before and (b) after using of CMOF-801(ASP) chiral catalyst for nitroaldole reaction.

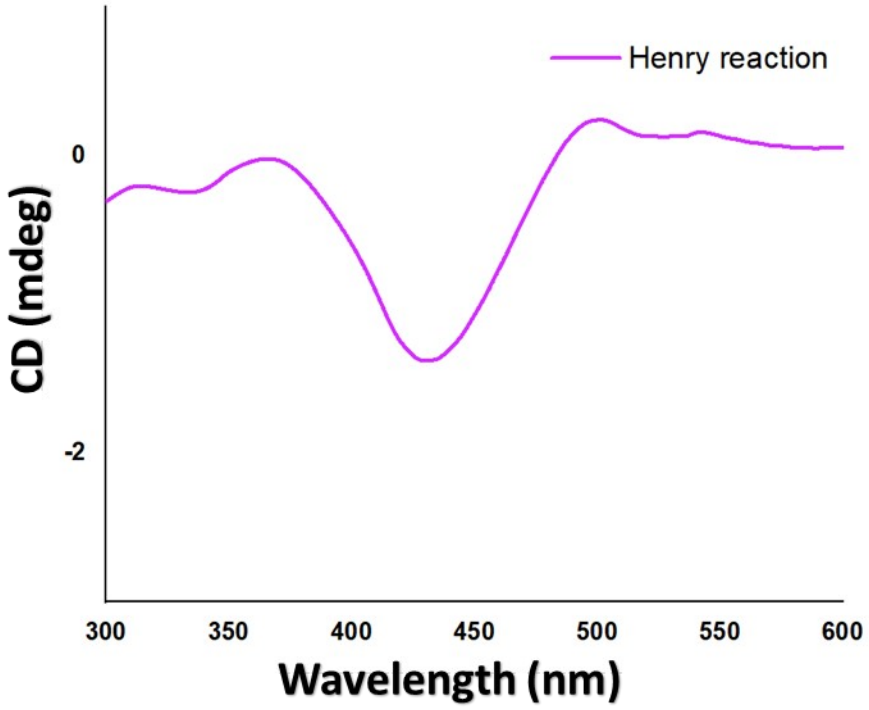

Figure S24. Circular dichroism for characterization of major enantiomer for the Henry reaction.

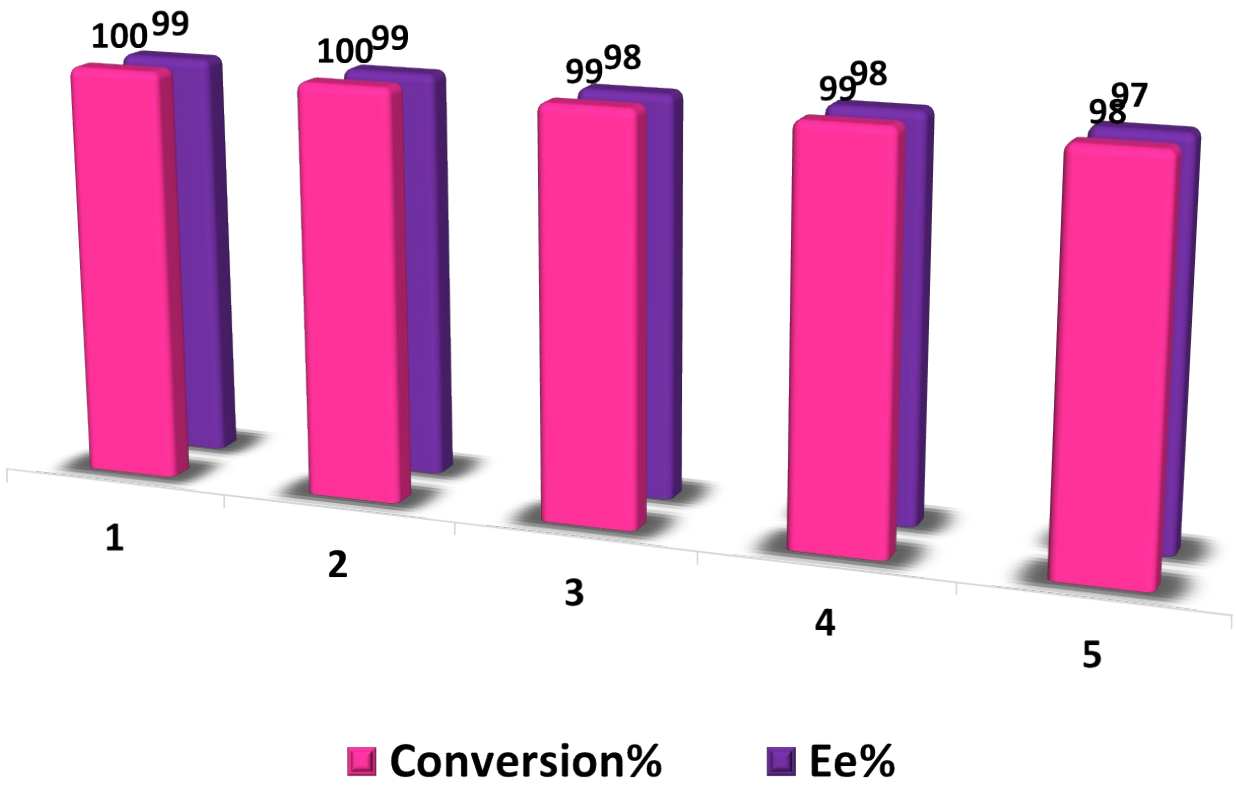

Figure S25. Reusability tests of CMOF-801(ASP) for Henry reaction.

Figure S26. ^{1}H NMR of 2-Nitro-1-phenylethan-1-ol in D_2SO_4.

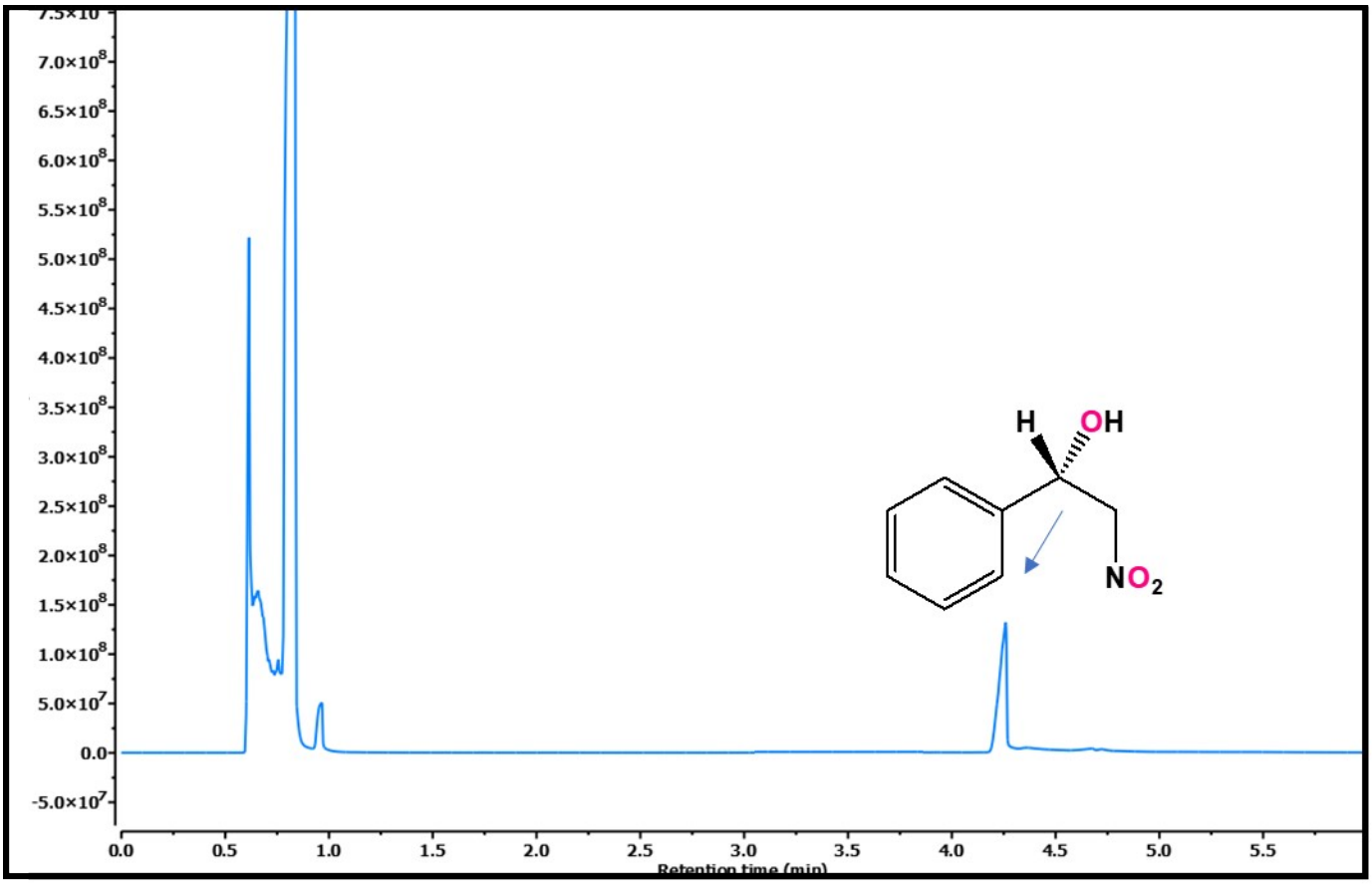

Figure S27. GC chromatogram for the Henry reaction catalyzed by CMOF-801(ASP).

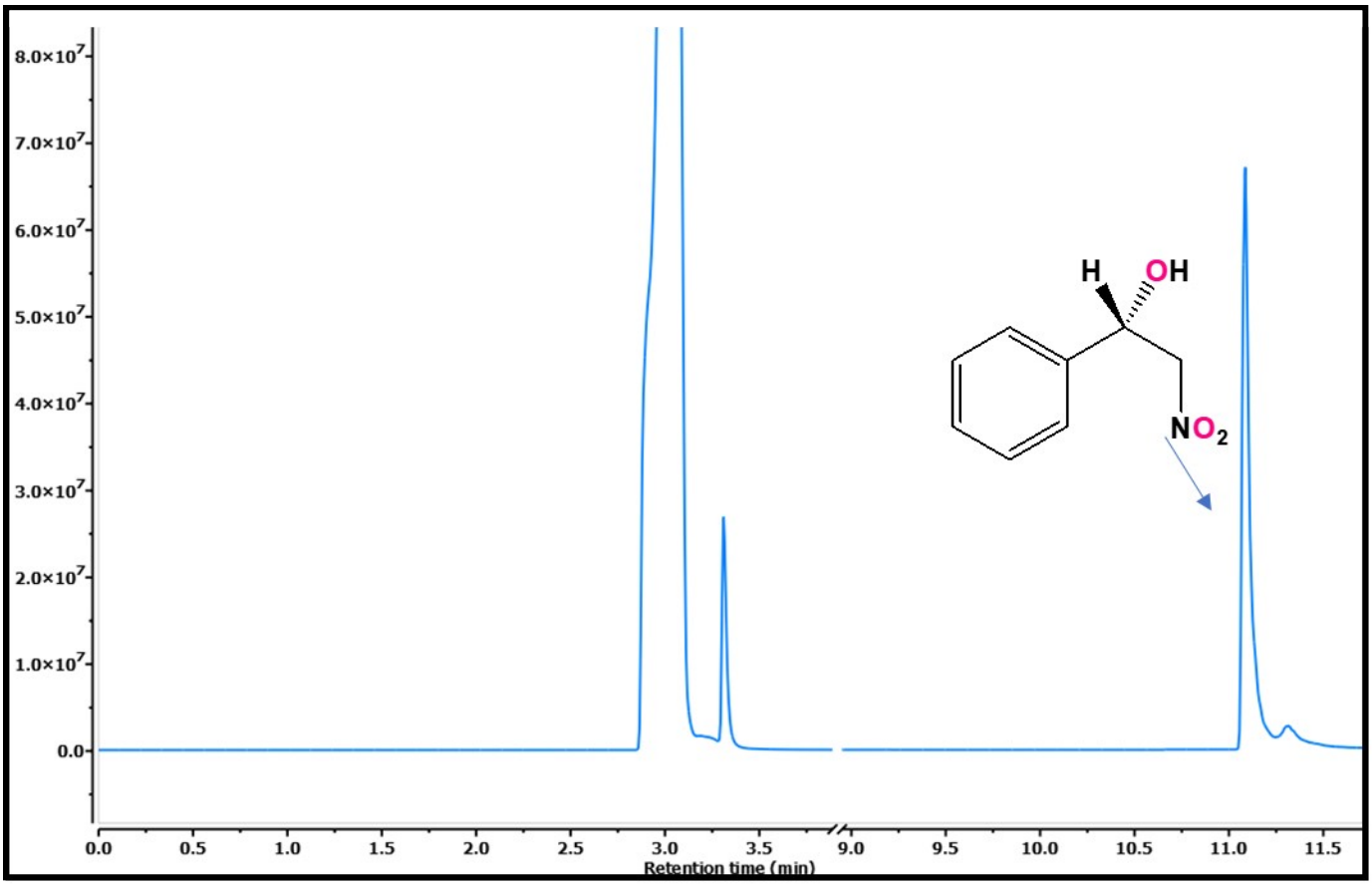

Figure S28. Chiral GC chromatogram for the ring-opening of styrene epoxide catalyzed by CMOF-801(ASP)

Table S6. Comparison of CMOF-801-(ASP) with other catalysts Henry reaction.

Entry	Catalyst	Temp (ºC)	Time	Yield (%)	Ref.
1	**Zn-MOF**	70	48h	84	6
2	**Cd-MOF**	R.T	72h	89	7
3	**Sm-MOF**	70	36h	43	8
4	**[Cd2(Cu(salen)-MOF**	R.T	48h	31	9
5	**Pd@DP-ZIF67/CalA**	R.T	20h	96	10
6	**MOF-801(P)**	R.T	15 minuets	8	**This work**
7	**MOF-801(D)**	R.T	15 minuets	80	**This work**
8	**MOF-801(ASP)**	R.T	15 minuets	100	**This work**

Section S5. Oxazolidinone formation reaction Characterization

Table S7. Optimization reaction condition for Oxazolidinone formation

Entry	Catalyst	Temperature (ºC)	Time (hour)	Pressure (atm)	Conversion (%)	Ee (%)
1	MOF-801(P)	90	12	1	15	-
3	MOF-801(D)	90	12	1	20	-
4	CMOF-801(ASP-25)	90	12	1	76	S
4	CMOF-801(ASP)	90	12	1	90	S
5	Fumaric acid	90	12	1	N.R	-
6	L-Aspartic acid	90	12	1	N.R	S
7	$ZrCl_4$	90	12	1	N.R	-
8	Physical mixture of L-ASP& $ZrCl_4$	90	12	1	7	-

Table S8. Reaction scope for the three-component cycloaddition of CO_2 with aromatic amines and substituted epoxides in the presence of CMOF-801(ASP) as a heterogeneous catalyst[a]

Entry	Aromatic amine	Epoxide	Product	Conversion (%)[b]
1	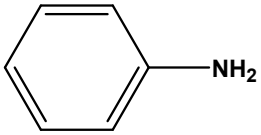	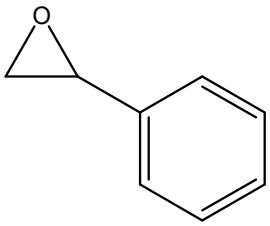	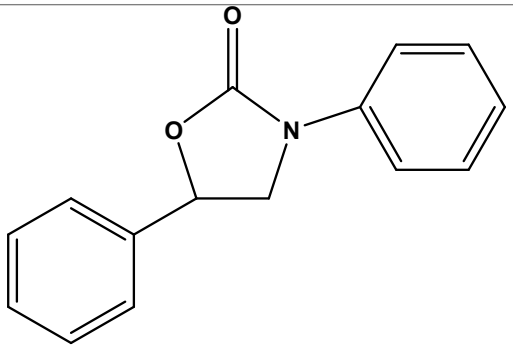	90
2	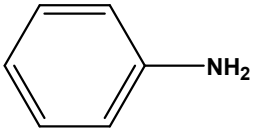	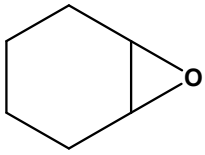	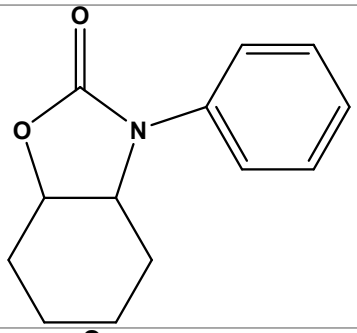	72
3	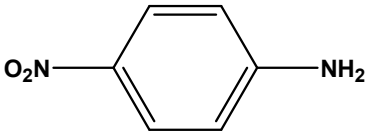	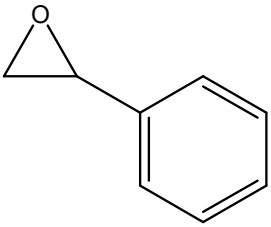	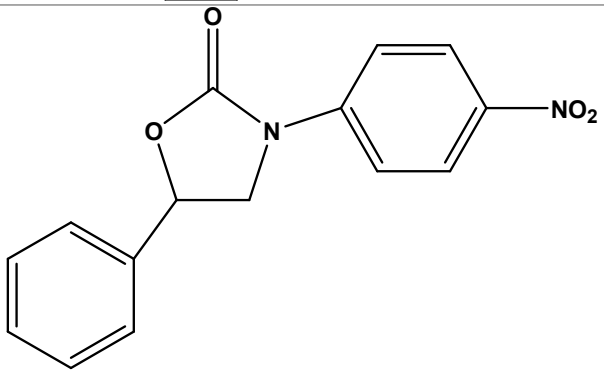	92
4	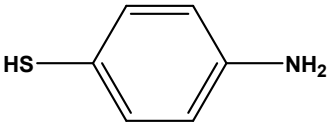	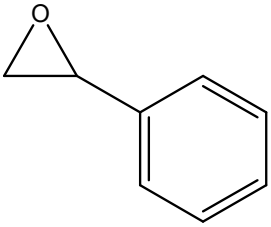	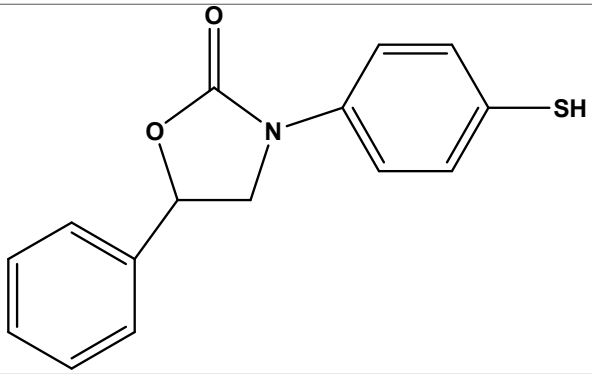	83

[a] Reaction conditions: epoxide (6.0 mmol), aromatic amine (2.0 mmol), CO_2 (1 bar), CMOF-801(ASP) catalyst (50 mg), solvent-free, 12 h, 90 °C.

[b] Isolated yield calculated with respect to aromatic amine as determined by GC

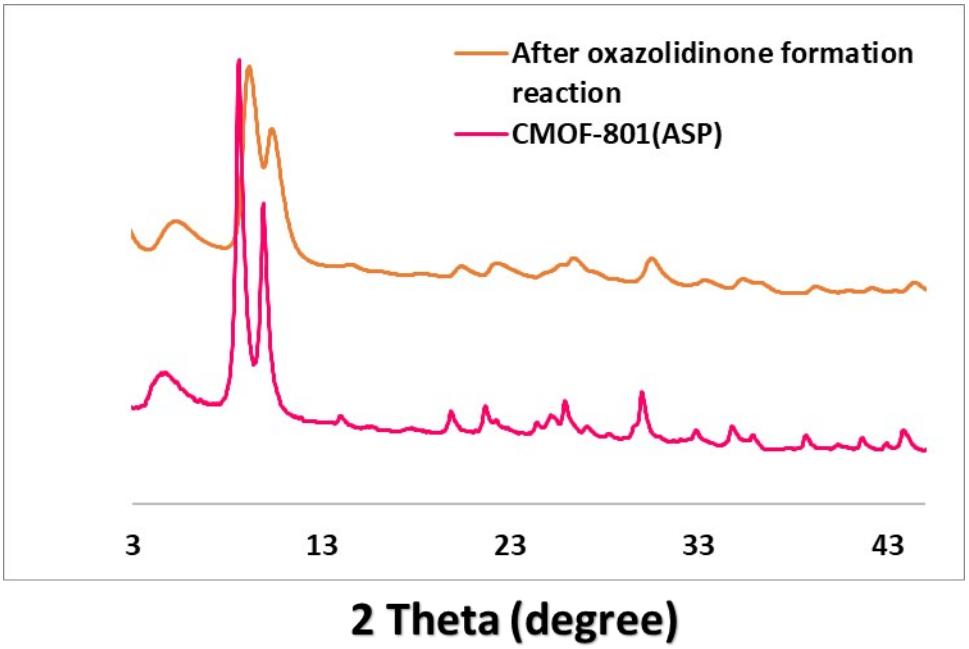

Figure S29. PXRD pattern comparison before and after using of CMOF-801(ASP) chiral catalyst for oxazolidine formation reaction.

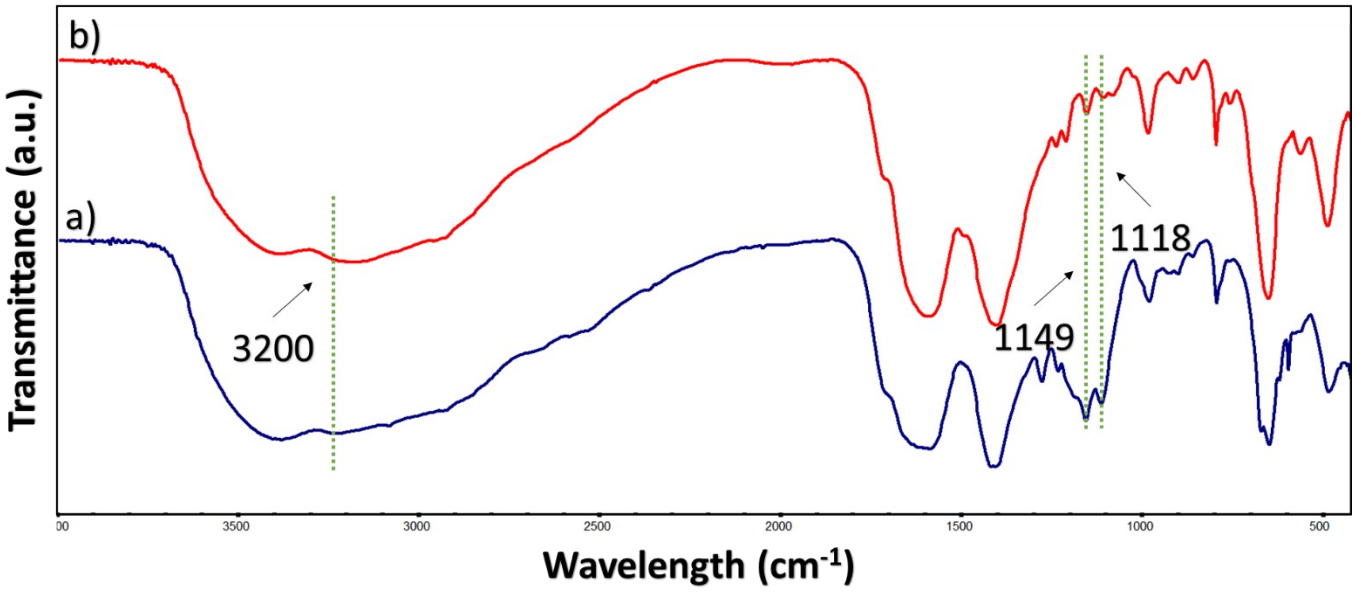

Figure S30. FTIR spectrum comparison (a) before and (b) after using of CMOF-801(ASP) chiral catalyst for oxazolidinone formation reaction.

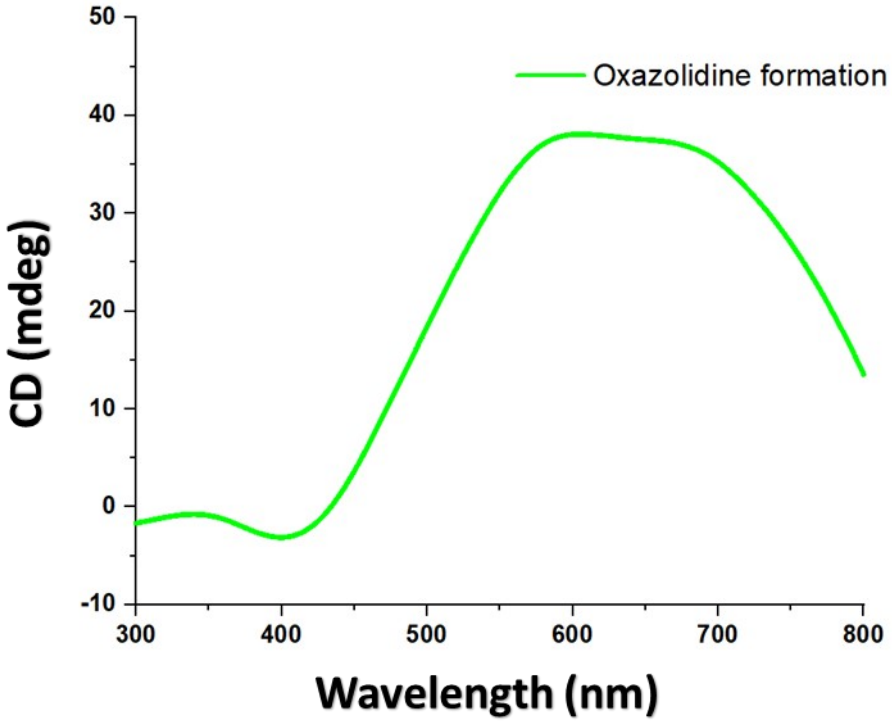

Figure S31. Circular dichroism for characterization of major enantiomer for the oxazolidinones formation reaction.

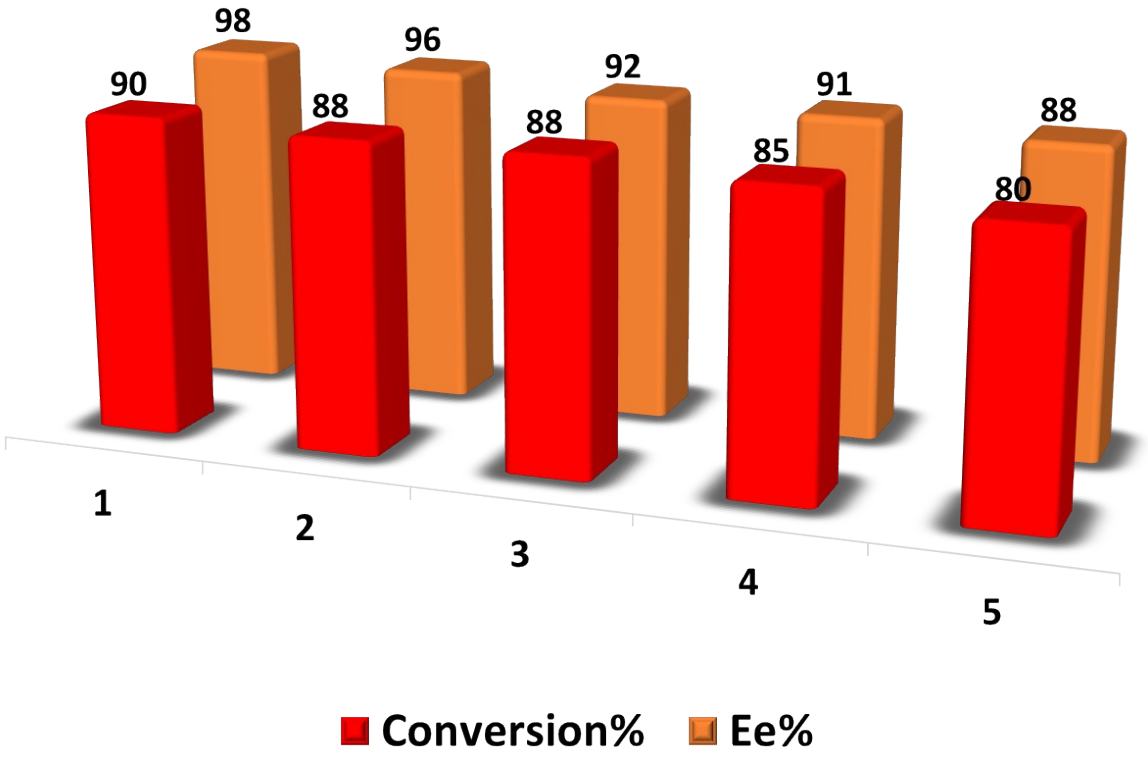

Figure S32. Reusability tests of CMOF-801(ASP) for oxazolidinone formation reaction.

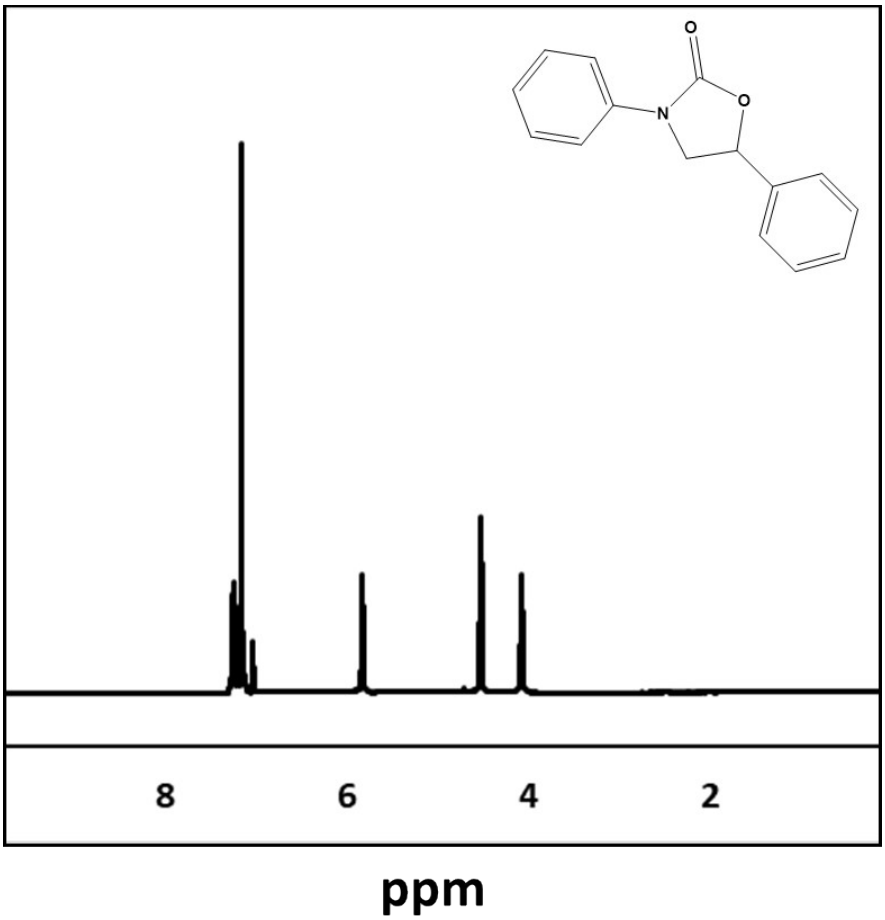

Figure S33. ^{1}H NMR of 3,5-diphenyloxazolidin-2-one.

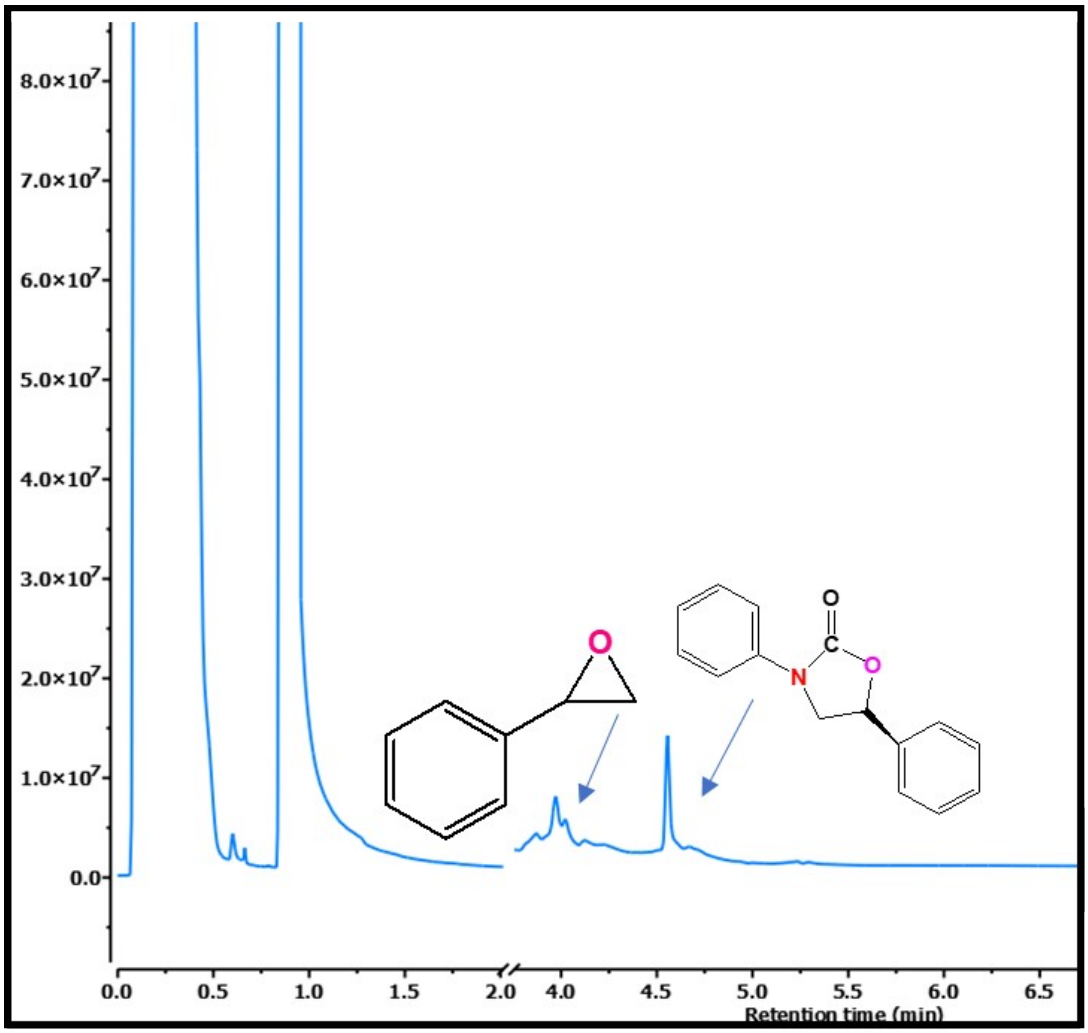

Figure S34. GC chromatogram for the oxazolidinone conversion though cycloaddition of CO_2 into styrene epoxide catalyzed by CMOF-801(ASP).

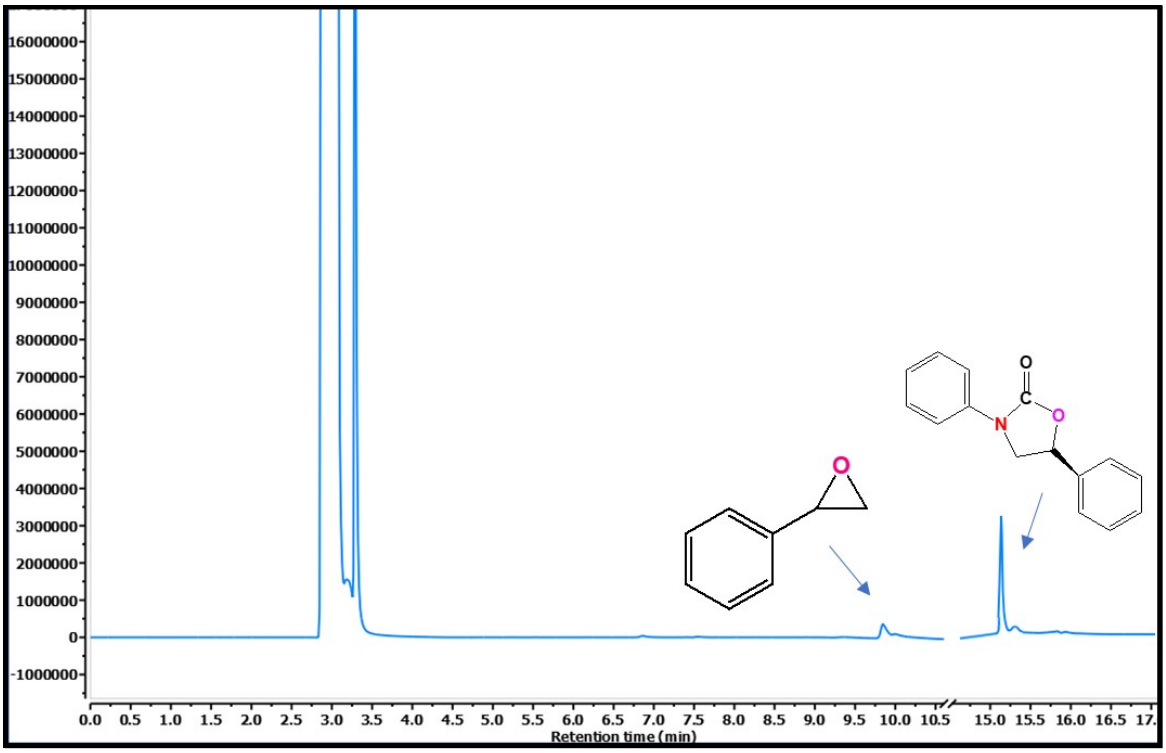

Figure S35. Chiral GC chromatogram for the oxazolidinone conversion though cycloaddition of CO_2 into styrene epoxide catalyzed by CMOF-801(ASP).

Table S9. Comparison of CMOF-801-(ASP) with other catalysts in oxazolidine formation reaction.

Entry	Catalyst	Temp (ºC)	Press (bar)	Time (hour)	Co-catalyst	Yield (%)	Ref.
1	**Ni-MOF**	90	1	12	TBAI	78	11
2	**UiO-66**	85	1	12	-	78	12
3	**MOF-801(P)**	90	1	12	-	7	**This work**
4	**MOF-801(D)**	90	1	12	-	20	**This work**
5	**CMOF-801(ASP)**	90	1	12	-	90	**This work**

References:

(1) Wang, S.; Wahiduzzaman, M.; Davis, L.; Tissot, A.; Shepard, W.; Marrot, J.; Martineau-Corcos, C.; Hamdane, D.; Maurin, G.; Devautour-Vinot, S. A Robust Zirconium Amino Acid Metal-Organic Framework for Proton Conduction. *Nature communications* **2018**, *9* (1), 1–8.

(2) Zhao, H.; Yi, B.; Si, X.; Cao, L.; Su, L.; Wang, Y.; Chou, L.-Y.; Xie, J. Solid-State Synthesis of Defect-Rich Zr-UiO-66 Metal–Organic Framework Nanoparticles for the Catalytic Ring Opening of Epoxides with Alcohols. *ACS Applied Nano Materials* **2021**, *4* (9), 9752–9759.

(3) Tanaka, K.; Otani, K. I.; Murase, T.; Nishihote, S.; Urbanczyk-Lipkowska, Z. Enantioselective Ring-Opening Reaction of Epoxides with MeOH Catalyzed by Homochiral Metal-Organic Framework. *Bulletin of the Chemical Society of Japan* **2012**, *85* (6), 709–714. https://doi.org/10.1246/bcsj.20110392.

(4) Tanaka, K.; Otani, K. Asymmetric Alcoholytic Kinetic Resolution of Styrene Oxide Catalysed by Chiral Metal–Organic Framework Crystals. *New Journal of Chemistry* **2010**, *34* (11), 2389–2391. https://doi.org/10.1039/C0NJ00038H.

(5) Gharib, M.; Esrafili, L.; Morsali, A.; Retailleau, P. Solvent-Assisted Ligand Exchange (SALE) for the Enhancement of Epoxide Ring-Opening Reaction Catalysis Based on Three Amide-Functionalized Metal–Organic Frameworks. *Dalton Transactions* **2019**, *48* (24), 8803–8814.

(6) Karmakar, A.; Guedes da Silva, M. F. C.; Pombeiro, A. J. L. Zinc Metal–Organic Frameworks: Efficient Catalysts for the Diastereoselective Henry Reaction and Transesterification. *Dalton Transactions* **2014**, *43* (21), 7795–7810. https://doi.org/10.1039/C4DT00219A.

(7) Ugale, B.; Dhankhar, S. S.; Nagaraja, C. M. Construction of 3D Homochiral Metal–Organic Frameworks (MOFs) of Cd(Ii): Selective CO2 Adsorption and Catalytic Properties for the Knoevenagel and Henry Reaction. *Inorganic Chemistry Frontiers* **2017**, *4* (2), 348–359. https://doi.org/10.1039/C6QI00506C.

(8) Prestipino, C.; Regli, L.; Vitillo, J. G.; Bonino, F.; Damin, A.; Lamberti, C.; Zecchina, A.; Solari, P. L.; Kongshaug, K. O.; Bordiga, S. Local Structure of Framework Cu (II) in HKUST-1 Metallorganic Framework: Spectroscopic Characterization upon Activation and Interaction with Adsorbates. *Chemistry of materials* **2006**, *18* (5), 1337–1346.

(9) Fan, Y.; Ren, Y.; Li, J.; Yue, C.; Jiang, H. Enhanced Activity and Enantioselectivity of Henry Reaction by the Postsynthetic Reduction Modification for a Chiral Cu(Salen)-Based Metal–Organic Framework. *Inorganic Chemistry* **2018**, *57* (19), 11986–11994. https://doi.org/10.1021/acs.inorgchem.8b01551.

(10) Dutta, S.; Kumari, N.; Dubbu, S.; Jang, S. W.; Kumar, A.; Ohtsu, H.; Kim, J.; Cho, S. H.; Kawano, M.; Lee, I. S. Highly Mesoporous Metal-Organic Frameworks as Synergistic Multimodal Catalytic Platforms for Divergent Cascade Reactions. *Angewandte Chemie International Edition* **2020**, *59* (9), 3416–3422.

https://doi.org/https://doi.org/10.1002/anie.201916578.

(11) Helal, A.; Fettouhi, M.; Arafat, M. E.; Khan, M. Y.; Sanhoob, M. A. Nickel Based Metal-Organic Framework as Catalyst for Chemical Fixation of CO2 in Oxazolidinone Synthesis. *Journal of CO2 Utilization* **2021**, *50*, 101603.

(12) Helal, A.; Cordova, K. E.; Arafat, M. E.; Usman, M.; Yamani, Z. H. Defect-Engineering a Metal-Organic Framework for CO2fixation in the Synthesis of Bioactive Oxazolidinones. *Inorganic Chemistry Frontiers* **2020**, *7* (19), 3571–3577. https://doi.org/10.1039/d0qi00496k.